Title

Endothelial Trauma Depends on Surface Charge and Extracellular Calcium Levels

Authors

Jade H. Cleary[1], Kara J. Wentzel[1], Abigail J. Howard[1], Adrian M. Sackheim[1], Sophia H. Piffard[1], J. Cory Benson[2], Grant Hennig[4], Dev Majumdar[3], Mohamed Trebak[2], Mark T. Nelson[4,5], Kalev Freeman[1,4]

Affiliations

Departments of [1]Emergency Medicine, [3]Surgery, and [4]Pharmacology, University of Vermont, Burlington VT; [2]Department of Pharmacology and Chemical Biology and Vascular Medicine Institute, University of Pittsburgh, Pittsburg PA; [5]Division of Cardiovascular Sciences, University of Manchester, Manchester UK

Corresponding Author

Kalev Freeman, Kalev.Freeman@med.uvm.edu, 802-338-1622

Sources of Support

NIH/NIGMS R35 GM144099, P20 GM125498 and P20 GM135007 (Core C: Cus- tomized Physiology and Imaging Core); NIH/NHLBI R35 HL140027, R35 HL150778 and R01 HL166944; NIH/NIA/NINDS RF NS128963, R01 NS110656, and R01 NS119971; NIH Office of the Director (S10-OD026843); European Union Horizon 2020 Research and Innovation Programme Grant Agreement 666881; Leducq Foundation Transatlantic Network of Excellence, Stroke-IMPaCT 19CVD01; the Totman Medical Research Trust.

Conflicts of Interest

There are no conflicts of interest for any of the authors.

Significance

In acute critical illness, the rapid collapse of vascular endothelial functions drives aberrant blood clotting and organ failure through mechanisms that are not understood. The recent breakthrough in transfusion medicine showing that administration of donor plasma improves survival of trauma patients has transformed the massive transfusion protocols used in surgical settings, but the sodium citrate used to prevent coagulation often produces significant and severe hypocalcemia. Here, we demonstrate that cytotoxic trauma factors that are elevated in the blood during resuscitation bind endothelial cell phospholipids, and that low Ca^{2+} exacerbates toxicity by increasing this interaction. These experiments lead to our surprising discovery of unexpected endothelial cell membrane theatrics that occur in response to injury, with direct visualization of fast plasma membrane movements and the release and reuptake of extracellular vesicles. These findings provide important insights into the nature of shock-induced endotheliopathy and highlight the potential cardiovascular risk associated with chelation-induced hypocalcemia during resuscitation.

Abstract

We hypothesized that cationic histones bind to endothelial cell membranes through electrostatic interactions with negatively charged phospholipids, and consequently, that low Ca^{2+} exacerbates toxicity by increasing binding and uptake of histones into cells. The role of the ubiquitous store-operated Ca^{2+} entry (SOCE) in histone responses is also unknown. Here, studying endothelial cells in surgical preparations and in culture, we observed clinically relevant histone concentrations, produced fast plasma membrane movements including vesiculation, blebbing, ruffling, and cellular collapse. The cell membrane theatrics observed were markedly different from the uniform pattern of exocytosis and blebbing produced by calcium overload with ionomycin. Interestingly, membrane permeabilization produced by histones (and not ionomycin) was transient and a subset of cells recovered membrane integrity within 1 hour. A role for SOCE in histone responses was ruled out by genetic ablation of the ORAI1/2/3 channel trio. Removal of extracellular Ca^{2+} prevented histone-induced intracellular Ca^{2+} overload while surprisingly exacerbating plasma membrane deformation. Conversely, decreasing the density of the negative charge surface by

adding calcium or multivalent cations gadolinium or increasing extracellular Ca^{2+} levels effectively screened common membrane phospholipids from interactions with labeled histones and prevented endothelial damage in cells exposed to histones. Collectively, these results indicate that low extracellular Ca^{2+} levels enhance interactions between histones and endothelial cell membrane phospholipids to increase cytotoxicity. Importantly, this supports the concept of aggressive Ca^{2+} repletion during resuscitation to prevent hypocalcemia, stabilize the endothelial cell membranes and improve cardiovascular recovery from shock.

Introduction

Cardiovascular shock secondary to trauma and sepsis is among the most common causes of morbidity and mortality worldwide[1,2]. Over 60 trillion interconnected vascular endothelial cells (ECs) connect all organs and regulate function in the body[3]. The sudden and devastating disruption of endothelial function that occurs locally and in distant organs after a severe insult, disrupting blood clotting, barrier function, and blood flow, known as shock-induced endotheliopathy, is a common denominator of acute critical illness that drives progressive organ failure and mortality[4–6]. Despite the emerging consensus that the release of cytotoxic histone proteins into the bloodstream, both from injured cells and activated neutrophils in the form of extracellular traps, is the inciting event that drives acute endothelial injury in trauma and severe infection[7–13], there are no proven treatments, and the fundamental mechanisms that underlie endothelial cell responses to severe injury remain largely unknown.

The results of clinical trials showing that the rapid transfusion healthy donor plasma to in the early prehospital setting (before arrival to the hospital) decreases biomarkers of endothelial injury and improves the survival of severely injured patients has transformed the emergency care of surgical trauma, and clinical protocols used at trauma centers for massive transfusion of blood products are evolving to these changes. Hypocalcemia is a common complication during the resuscitation of critically injured patients, resulting from factors including the infusion of blood products containing sodium citrate (which has an anticoagulant effect by chelating Ca^{2+} ions), hypoperfusion, and decreased hepatic clearance of the citrate due to impaired perfusion[13]. Low plasma Ca^{2+} levels in trauma are predictive of mortality and need for

79 multiple transfusions[14,15]. Despite the prevalence of hypocalcemia in trauma patients, there is controversy
80 regarding the appropriate thresholds, timing and extent of Ca^{2+} administration used for massive transfusion
81 protocols[16,17].

82 Here, we hypothesized that cationic histones interact electrostatically s with negatively charged
83 phospholipids, and consequently, that low Ca^{2+} exacerbates toxicity by increasing binding of histones to
84 cell membranes. We studied ECs both in culture and in surgically opened vascular preparations using live
85 cell video microscopy, to address the following questions: (1) Are histone-induced Ca^{2+} oscillations SOCE-
86 dependent? (2) Is Ca^{2+} influx necessary for histone-induced toxicity? (3) Do extracellular Ca^{2+} levels
87 modulate the membrane effects of histones? (4) To what extent are histone-induced membrane changes
88 dependent on the negative charge density of the local electric field near the cell surface?

89

90 **Results**

91 **Gadolinium prevents histone-induced endothelial cell calcium events.** To establish the contribution
92 of SOCE to Ca^{2+} elevations, we first employed a pharmacological approach using Gd^{3+}, a trivalent
93 lanthanide that is useful when applied at low concentrations (<10 μM) as a SOCE inhibitor[18]. Freshly
94 harvested murine mesenteric arteries, surgically opened to expose the endothelium, were loaded with a
95 fluorescent Ca^{2+} indicator and exposed to clinically relevant concentrations of histones (50 μg/mL) with
96 Ca2+ (1.2 mM) in the presence or absence of Gd^{3+} (10 μM) (Figure 1 A-C, Supplemental Videos 1 and 2).
97 Rapid (<5 minutes) and irregular increases in endothelial cell Ca^{2+} fluorescence were observed as
98 expected. Surprisingly, these effects were completely blocked if histones were applied following pre-
99 treatment, but not after, with Gd^{3+}.

100 These Ca^{2+} oscillations were recapitulated in HEK-293 cells loaded with the ratiometric Ca^{2+}
101 indicator Fura-2 and stimulated with increasing concentrations of histones. Ca^{2+} signals were present in
102 response to histones starting at concentrations of 25 μg/mL, and high amplitude, frequent calcium
103 oscillations were observed in response to 50 μg/mL of histones (Figure 1 D,E). As we previously
104 demonstrated in surgical vascular EC preparations[11], extracellular Ca^{2+} is necessary for histone-induced
105 Ca^{2+} events. When HEK-293s were exposed to histones (50 μg/mL) in a solution of 0 mM Ca^{2+}, no Ca^{2+}

106 activity was observed. After 5 minutes, the extracellular solution was replaced with 2 mM Ca^{2+} and a
107 significant increase in activity immediately after the extracellular Ca^{2+} levels were restored. Similar to our
108 findings in ECs, we found that pre-treatment with Gd^{3+} (10 μM) completely blocked histone-induced Ca^{2+}
109 signals in HEK-293s (Figure 1 D,F). Interestingly, post-treatment with Gd^{3+} (10 μM) within 5 minutes of
110 histone (50 μg/mL) exposure was unable to quench histone-induced Ca^{2+} influx (Figure 1 D,G). We
111 additionally tested a lower concentration of Gd^{3+} (5 μM) which should be effective at inhibition of SOCE-
112 dependent Ca^{2+} activity[18]. In contrast to the complete block achieved by 10 μM Gd^{3+}, this lower
113 concentration was unable to inhibit histone-induced Ca^{2+} increases in either pre-treatment or post-
114 treatment conditions (Supplemental Figure 1A,B).

115 **Store operated calcium entry is not required for histone-induced calcium events.** Since
116 pharmacological approaches to blocking SOCE, such as Gd^{3+}, can have non-selective effects on other
117 cation channels, we applied a complementary genetic approach[19]. ORAI channels are key mediators of
118 SOCE through their binding to STIM1, and knocking out all three ORAI homologs completely prevents
119 functional SOCE responses[19–21]. We therefore utilized ORAI triple knockout (TKO) HEK293 cells to
120 determine the role of SOCE in histone-mediated Ca^{2+} signals[18]. While the blockade of histone responses
121 by Gd3+ (Fig 1A-C) had suggested a role for ORAI channels, surprisingly, there was no apparent difference
122 in histone-induced Ca^{2+} activity between wildtype and ORAI-TKO HEK-293 cells (Figure 1D-G). These
123 results effectively rule out ORAI channels as a contributor to histone-induced Ca^{2+} influx in ECs, and forced
124 us to reassess the Gd^{3+} results. Since the inhibitory activity of Gd^{3+} for SOCE is in the nM range, with an
125 IC50 of less than 100nM[22], and 5 μM Gd^{3+} pre-treatment was insufficient to achieve a complete block of
126 histone-induced Ca^{2+} signals (Supplemental Figure 1), we therefore concluded that the Gd^{3+} effect must
127 be due to a mechanism of action independent of SOCE.

128 **Histones bind and deform endothelial cell plasma membranes.** Because histones-induced Ca^{2+} entry
129 was independent of ORAI channels, but blocked by 10 μM Gd^{3+}, we reasoned that the Gd^{3+} may be acting
130 via a surface charge screening effect. Multivalent cations such as Gd^{3+} can neutralize the negative charge
131 at the membrane surface, altering the local electric field near the membrane, thereby shielding the plasma
132 membrane lipids. Preventing histones from binding directly to the plasma membrane might prevent

133 localized membrane injury or pore-formation that allows entry of extracellular Ca^{2+}. To evaluate the impact
134 of histones on plasma membrane structure and morphology in ECs, we performed electron microscopy on
135 *en face* murine mesenteric arteries following stimulation with histones (50 µg/mL) for 30 minutes in HEPES-
136 PSS. We found that untreated arteries appeared to have intact cell-to-cell junctions and a flat, uniform cell
137 morphology. The plasma membranes appeared smooth and minimal extracellular debris or vesicles were
138 noted (Figure 2A). In contrast, ex vivo ECs treated with histones showed significant alterations in cell
139 morphology. Cells appeared to have retracted, causing a breakdown of cell-to-cell junctions and the
140 exposure of retraction fibers. Numerous blebs and extracellular vesicles were also visible on histone-
141 treated cells (Figure 2A).

142 Due to the dramatic membrane changes seen on electron microscopy, we next wanted to elucidate
143 the dynamic effect of histones on the endothelial cell plasma membrane. The styryl pyridinium dye FM1-
144 43, which fluoresces when inserted in lipid bilayers, was used to stain the plasma membranes of histone-
145 stimulated ECs. Furthermore, FM1-43 can also reveal cell membrane disruption and permeability. While
146 normally impermeable to cells, FM1-43 floods the cytoplasm and stains internal membrane structures of
147 damaged cells[23]. We compared the membrane effects of histones to those of ionomycin at a concentration
148 sufficient to both mobilize intracellular stores and produce sustained Ca^{2+} influx[24]. Both stimuli resulted in
149 cellular blebbing and membrane permeability over a period of 40 minutes, but the pattern and
150 characteristics of plasma membrane responses to these stimuli were markedly different (Supplemental
151 Videos 3 and 4). The endothelial response to ionomycin was characterized by synchronized cytoplasmic
152 filling of the membrane dye between 20 minutes to 30 minutes of exposure, culminating in 92% (± 12%) of
153 cells showing a 2-fold or greater increase in fluorescence at 40 minutes. In comparison, the endothelial
154 response to histones also showed membrane dye internalization within 40 minutes of exposure, but in a
155 different pattern. Most importantly, histone exposure resulted in extensive FM1-43 dye uptake in only a
156 subset of ECs 34% (± 7%) within 40 minutes at normal Ca^{2+} levels (1.2 mM). The timing of dye entry was
157 also not uniform across cells, instead occurring in a few cells at a time over the course of 10 to 20 minutes.
158 The peak timing of the membrane changes (~30-40 minutes) was much later than when we observed the
159 Ca^{2+} surges (~3-5 minutes). We also noted that dye uptake originated from hotspots within a single cell

160 then spreads to the rest of the cytoplasm. After initial dye uptake in these hot spots, FM1-43 staining
161 spreads from the outer membrane to internal membrane components, until the entire cell cytoplasm is
162 rapidly filled with dye while the nucleus remains unstained. In the remaining ~ ⅔ of cells, there were either
163 no changes in cell permeability or dye entry was sequestered to hot spots within cell protrusions without
164 progressing further.

165 Close inspection of the video recordings demonstrated fast plasma membrane movements and
166 release of extracellular vesicles in response to both ionomycin and histone, but different patterns of
167 responses were evident. To compare the patterns of membrane changes, we present two dramatic
168 examples of fields of endothelial cells recorded over 1 hour with zoomed-in regions of interest, in order to
169 demonstrate specific features (Figure 3). The patterns of membrane movements caused by ionomycin
170 included extension of filopodia and blebbing (Figure 3A, Supplemental Videos 5, 6). Histone exposure
171 resulted in dynamic cell responses in a different pattern. Membrane movements produced by histones and
172 not ionomycin included cell rounding with exposure of retraction fibers and ruffling sheets of plasma
173 membrane at the edges of cells particularly at surfaces near adjacent cells (Figure 3B, Supplemental
174 Videos 7, 8). Histone exposure also resulted in an end-stage pattern of blebbing and cessation of cell
175 movements in some cells(Figure 3B, Supplemental Videos 9). Additional examples of histone-induced
176 plasma membrane ruffling and blebbing are also provided (Supplemental Videos 10, 11).

177 The patterns of EV release produced by histones and ionomycin was also different. Histone-
178 induced membrane fragments showed a wide range of sizes, including large fragments consistent with
179 apoptotic bodies (Supplemental Video 4). In contrast, the endothelial response to ionomycin was disticn
180 resulted in the synchronous appearance of punctate, stippled, rapidly vibrating symmetrical membrane
181 particles <5 μm. In some cases, extracellular vesicles were visualized being released by cells absorbed
182 by both adjacent and remote cells, surfing on nanotubes, or passed between cells directly across
183 connected lamellipodia (Supplemental Video 12).

184 **Plasma membrane changes are not due to calcium overload.** Based upon the earlier and more rapid
185 occurrence of histone-induced endothelial cell Ca^{2+} influx than plasma membrane changes, we considered
186 the possibility that Ca^{2+} overload was the trigger for subsequent membrane disruption. We previously

187 established extracellular Ca^{2+} is required for histone-induced intracellular Ca^{2+} entry into vascular
188 endothelial cells[11], so we reasoned that, if histone-induced endothelial cell Ca^{2+} overload drives cell
189 membrane changes, the removal of extracellular Ca^{2+} should prevent the membrane responses. We
190 therefore tested the impact of low Ca^{2+} on histone-induced endothelial cell membrane responses visualized
191 with FM1-43. Surprisingly, exposure to histones in low Ca^{2+} exhibited an exaggerated response compared
192 to normal extracellular Ca^{2+} conditions (1.2 mM). While histone-exposure caused significant dye uptake in
193 33.6% (± 6.8%) of cells 1.2 mM Ca^{2+} levels, this value increased to 60.1% (± 11.3%) of cells at 0 mM Ca^{2+}
194 concentrations. Similarly, the average highest change in fluorescence at 40 minutes increased from 6.56
195 AU at 1.2 mM Ca^{2+} to 18.72 AU at 0 mM Ca^{2+} (Figure 4). Furthermore, the pattern of cell membrane
196 deformation produced by histones under low Ca^{2+} was similar to that produced in normal Ca^{2+} containing
197 solutions, but with more extensive of membrane thickening, blebbing, and release of membrane fragments
198 (Figures 3-4).

199 **Neutralizing cell membrane surface charge prevents histone interactions.** We then investigated the
200 impact of high Ca^{2+} and Gd^{3+} on histone-induced membrane disruption in live ECs. Both high Ca^{2+} (12 mM)
201 and Gd^{3+} (10 μM) were protective. The fast plasma membrane movement and deformation produced by
202 histones was markedly diminished in the presence of high Ca^{2+}, and pretreatment with Gd^{3+} rendered
203 histone-stimulated cells practically indistinguishable from unstimulated cells. Quantitative spatiotemporal
204 analysis of video recordings showed that high Ca^{2+} and Gd^{3+} prevented FM1-43 uptake into cells produced
205 by histones (Figure 4).

206 To confirm our microscopy findings, we used flow cytometry to quantify endothelial cell FM1-43
207 update after histone exposure under conditions of normal or high Ca^{2+} compared to Ca^{2+} free conditions.
208 Flow cytometry results recapitulated the pronounced internalization of FM1-43 in a subset of cells following
209 exposure to histones (50 μg/mL) in both normal and low Ca^{2+} conditions. The mean fluorescent intensity
210 (MFI) of FM1-43 increased 1.23-fold following histone exposure in 1.2 mM Ca^{2+} and 1.33-fold in 0 mM
211 Ca^{2+}. Conversely, cells stimulated with histones in 12 mM Ca^{2+} showed a 1.36-fold decrease in MFI relative
212 to unstimulated cells at the same Ca^{2+} concentration (Figure 5A). These findings further support that

213 histone interactions with endothelial cell membranes can be modulated by extracellular Ca^{2+}
214 concentrations.

215 The pronounced effects of extracellular Ca^{2+} and Gd^{3+} on blocking histone cytotoxicity indicated
216 that histone-induced membrane effects depend on strength of the plasma membrane surface charge and
217 occur independently of SOCE and Ca^{2+} entry. Thus, we hypothesized that these cations protect ECs from
218 histones by directly neutralizing negatively-charged phospholipids and reducing electrostatic interactions
219 between histones and the plasma membrane. To test this, we measured the binding affinity of a tagged-
220 histone protein (GST-H3) to individual phospholipids found commonly in biological membranes in the
221 presence or absence of elevated Ca^{2+} or Gd^{3+}. Like prior studies[11], we observed that in the absence of
222 Ca^{2+}, histones strongly bind to anionic not zwitterionic membrane phospholipids, consistent with an
223 electrostatic interaction (Figure 5B,C). We found that Gd^{3+} (30 μM) completely blocked all histone-
224 phospholipid interactions, removing the preferential binding motifs. Similarly, high Ca^{2+} (12 mM)
225 significantly reduced histone binding to most phospholipids. Interestingly, the presence of Ca^{2+} appeared
226 to increase binding affinity for lysophosphocholine.

227 **Phosphatidyl serine translocation to external leaflet occurs in response to histone stimulation even**
228 **in the absence of external calcium.** Histone stimulation of endothelial cells promotes thrombosis in part
229 due to translocation of phosphatidyl serine (PS) to the membrane surface through a process that is
230 inhibited by blocking the calcium-activated phospholipid scramblase TMEM16F[26]. However, increased PS
231 on the external leaflet of the plasma membrane may also indicate programmed cell death, so it is not clear
232 if the Ca^{2+} overload produced by histones activated the scramblase directly to produce transient changes
233 in PS or if the cells were pre-apoptotic and destined for cell death. We were therefore interested to
234 determine whether histone-exposed PS translocation can be modulated by extracellular Ca^{2+}
235 concentrations, and the extent to which these cells also permeable to to the viability dye propidium iodide
236 (PI). Following 1 hour of histone exposure in HEPES-PSS containing varying concentrations of Ca^{2+} (0,
237 1.2, 12 mM), cells were stained with Annexin V for PS exposure and PI for permeability then evaluated by
238 flow cytometry. At a moderate histone dose of 50 μg/mL, cells at normal Ca^{2+} levels of 1.2 mM showed a
239 5-fold increase in PS^{+}/PI^{-} cells to 3.85% (± 0.22%) relative to unstimulated cells at the same Ca^{2+} level.

240 This percentage dropped to 2.73% (± 0.55%) at 0 mM Ca^{2+} and 1.16% (± 0.33%) at 12 mM Ca^{2+}, which
241 was almost identical to unstimulated cells at all Ca^{2+} levels (Supplemental Figure 2). Similarly, 50 µg/mL
242 histones resulted in 8.40% (± 1.69%) of cells that were double positive (PS^+/PI^+) at 1.2 mM Ca^{2+} which
243 represents a 2-fold increase relative to unstimulated cells. Like the PS^+/PI^- findings, this percentage
244 dropped to 6.19% (± 2.97%) at 0 mM Ca^{2+} concentrations. Notably, unstimulated cells in the 12 mM Ca^{2+}
245 condition showed an elevated PS^+/PI^+ percentage at 8.18% (± 0.28), matching the respective histone-
246 stimulated population of 8.29% (± 2.76%). Thus, high Ca^{2+} levels were protective from histone-induced
247 cytotoxicity, but caused increase PS exposure and PI uptake at baseline (Supplemental Figure 2).

248 Since 50 µg/mL of histones did not cause dramatic changes in PS exposure or PI uptake, we next
249 tested a higher dose of 100 µg/mL histones which we have previously shown was sufficient to produce PS
250 translocation in endothelial cells[26]. At this higher dose, 32.15% (± 7.37%) of cells were PS^+/PI^- at 1.2 mM
251 Ca^{2+} which dropped to 24.20% (± 4.95%) at 0 mM Ca^{2+} and 3.52% (± 1.32%) at 12 mM Ca^{2+}. When
252 compared to unstimulated controls at the various Ca^{2+} levels, these changes represent 16-fold, 14-fold,
253 and 1.5-fold increases in PS^+/PI^- percentages for 1.2 mM Ca^{2+}, 0 mM Ca^{2+}, and 12 mM levels, respectively.
254 Similarly, the PS^+/PI^+ percentages were 13.38% (± 3.02%), 12.93% (± 1.82%), and 4.11% (± 1.05%)
255 following 1 hour of 100 µg/mL histone stimulation at 12 mM, 0 mM, and 12 mM Ca^{2+} concentrations,
256 respectively. Interestingly, since the percentage of PS^+/PI^+ cells in the unstimulated 12 mM Ca^{2+} condition
257 was elevated from 5.51% (± 1.01%) in normal Ca^{2+} to 8.14% (± 4.13%), the histone-stimulated cells at the
258 12 mM Ca^{2+} level appeared to have less cell death than their respective control. These results indicate that
259 both moderate and high doses of histones lead to both PS exposure and PI uptake in a subset of cells.

260 **Membrane permeabilization produced by histones is reversible.** Although these findings show that
261 high doses of histones can kill ECs, we also considered the possibility that a subset of PS-flipped and
262 permeabilized cells could recover their membrane integrity. Hence, we next sought to evaluate cell
263 recovery following histone-induced injury using a novel strategy involving live-cell imaging with different
264 colored viability dyes. Live ECs were initially stained with Hoechst nuclear dye and SYTOX Green to
265 determine baseline viability. The adherent monolayers were then washed multiple times to remove
266 unbound dye and subsequently incubated in HEPES-PSS containing no stimulant, histones (100 µg/mL),

267 or ionomycin (10 μM). Following 1 hour of stimulation, the cells were stained and imaged with SYTOX
268 Green again to determine post-stimulation viability. Finally, the cells were recovered in fresh DMEM with
269 10% FBS at 37 °C and 5% CO_2 for 3 hours then stained with red SYTOX AADvanced for post-recovery
270 viability (Figure 7A). Through this experimental design, we were able to use microscope filters to
271 distinguish between 4 distinct cell phenotypes: 1. Intact (blue alone), 2. Late Permeability (blue and red),
272 3. Sustained Permeability (blue, red, and green), and 4. Recovered (blue and green).

273 In the histone-treated group, a subset of cells exhibited early membrane permeability to SYTOX
274 Green, but excluded the red SYTOX AADvanced, indicating regained membrane integrity (Figure 7C,E).
275 In contrast, cells treated with ionomycin, a positive control, demonstrated sustained and uniform
276 permeability to both SYTOX Green and red SYTOX AADvanced, consistent with irreversible membrane
277 damage. Panel D shows cumulative permeability over time, based on the combined percentage of cells
278 positive for either dye at each timepoint. The increase in permeability observed in the histone group may
279 be partially influenced by variability in imaging fields across timepoints. Panel E quantifies the distribution
280 of cells in each condition according to dye uptake classification (as outlined in Panel A): SYTOX Green
281 only ("recovered"), SYTOX Green and red SYTOX AADvanced double-positive ("sustained permeability"),
282 or red SYTOX AADvanced only (not observed). At the final timepoint, 15.0% (± 2.9%) of histone-treated
283 cells were SYTOX Green-positive only, indicating recovery. Conversely, 41.5% (± 10.7%) were double-
284 positive, indicating sustained permeability. In the ionomycin-treated condition, 94.8% (± 2.6%) of cells were
285 double-positive, and 0% (± 0%) of cells had recovered membrane integrity. These results indicate that,
286 although histones are highly cytotoxic, a subset of permeabilized endothelial cells can repair their plasma
287 membranes and recover from histone exposure.

288

289 **Discussion**

290 The identification of endotheliopathy as a driver of coagulopathy and poor outcomes in shock states
291 of sepsis (e.g., bacterial infection, COVID-19) and trauma (e.g., hemorrhage, brain or multisystem injury,
292 burns)[9,27,28] was an important advance in critical care medicine. The paradigm of SHINE provides a unifying
293 pathophysiologic mechanism that explains how different shock states converge to produce similar patterns

294 of endothelial activation and injury[4,5]. In this study, we investigated mechanisms of histone-induced
295 endotheliopathy that demonstrate the importance of extracellular Ca^{2+} in shielding electronegative
296 endothelial cell surfaces from histone cytotoxicity. We have previously demonstrated that histones initiate
297 large EC Ca^{2+} oscillations that are pro-inflammatory, pro-thrombotic, and promote barrier breakdown[11,29,30].
298 Store-operated calcium entry (SOCE) is the most ubiquitous Ca^{2+} entry in non-excitable cells, such as ECs,
299 that is triggered in response to a variety of stimuli such as vascular endothelial growth factor (VEGF) and
300 thrombin[31]. This led to our initial hypothesis that SOCE contributes to histone-induced Ca^{2+} influx; however,
301 our experimental results did not support this model. We then considered an alternate hypothesis: histones
302 may induce Ca^{2+} entry by binding and deforming EC membranes, independently of SOCE. In addition, we
303 aimed to understand the extent to which intracellular Ca^{2+} overload drives histone toxicity[32–34]. We also
304 considered the possibility that removal of Ca^{2+} would increase exposure of negatively charged
305 phospholipids on EC membranes to interact with cationic histones while surface charge screening with the
306 addition of Ca^{2+} or multivalent cations would decrease this interaction. We report 4 novel findings: 1)
307 Activation of plasma membrane SOCE channels ORAI1/2/3 either directly or indirectly through release of
308 intracellular Ca^{2+} stores does *not* contribute to histone-induced cytosolic Ca^{2+} influx; 2) histones bind to
309 and deform ECs, producing fast irregular plasma membrane Ca^{2+} flickers or spikes in a pattern distinctly
310 different from the regenerative Ca^{2+} oscillations induced by physiological agonists[19] or the large plateaus
311 caused by ionomycin-induced Ca^{2+} influx; 3) Ca^{2+} influx is *not* required for histone-induced endothelial cell
312 deformation, and 4) histone-induced membrane permeability depends on electrostatic interactions with
313 negatively charged membrane phospholipids which are exacerbated by low Ca^{2+} and blocked by mM Ca^{2+}
314 or μM Gd^{3+}. These findings provide important insights into the nature of SHINE and highlight the potential
315 cardiovascular risk associated with hypocalcemia during resuscitation.

316 The release of intracellular Ca^{2+} stores and subsequent activation of ORAI channels is an important
317 mechanism for endothelial and immune cell signaling. Our initial experiments which showed that Gd^{3+}
318 blocked histone-induced endothelial cell Ca^{2+} influx (Figure 1) suggested SOCE may also play a role in
319 histone responses, as Gd^{3+} is a known ORAI channel antagonist[22]. However, we were surprised to discover
320 that the ablation of all three SOCE channels (ORAI1, ORAI2, and ORAI3) had no impact on histone-

321 induced endothelial cell Ca^{2+} overload (Figure 2). This effectively ruled out SOCE as a mechanism of
322 histone-induced Ca^{2+} signaling. Moreover, these results are consistent with recent observations that
323 histones and LPS activate ECs by distinct, additive pathways[30].

324 Our observation that histone-induced Ca^{2+} entry was independent of ORAI but blocked by Gd^{3+}
325 provided support for an alternate model in which histones allow direct entry of extracellular Ca^{2+} by creating
326 pores and deforming the outer membrane. We visualized the time course and extent of endothelial cell
327 membrane deformation produced by histone exposure at high spatial and temporal resolution for the first
328 time using video imaging of endothelial cell plasma membranes labeled with the fluorescent dye FM1-43.
329 This dye has been used to study endothelial cell membrane injury produced by other insults such as laser
330 injury[23,35], but we are not aware of prior studies using this dye to study histone responses. We found that,
331 indeed, histones deform endothelial cell membranes and produce a large increase in membrane
332 fluorescence within cells. Membrane dye uptake after histone exposure was statistically significant,
333 measured both by spatiotemporal analysis of video results and by separate flow cytometry experiments.

334 Utilizing both electron microscopy and live cell confocal microscopy, we identified novel patterns of
335 membrane dynamics in response to histones (Figure 3). First, we were surprised by the dramatic and fast
336 plasma membrane movements that histones produced, which included examples of 1) membrane ruffling,
337 2) blebbing of the cell surface, 3) release of cell membrane fragments, 4) retractions of lamellipodia, and
338 5) cellular collapse with rapid membrane dye internalization. Second, over a period of 40 minutes, only a
339 subset of approximately one-third to one-half of visible cells in each experiment responded to histones
340 while other cells appeared unaffected. Moreover, the pattern of membrane response even at the
341 subcellular level was not uniform, with membrane changes initially isolated to “hot spots” which spread
342 inward over several minutes until the entire cell rapidly filled with dye. In the remaining cells, there were
343 either no changes in cell permeability or dye entry was sequestered to hot spots within cell protrusions
344 without progressing further. This heterogeneity is consistent with other studies of histone responses in both
345 cultured cells and native endothelium, in which only a fraction of cells showed Ca^{2+} entry or PI uptake after
346 histone exposure[11]. Endothelial cell heterogeneity, even within a single blood vessel, has also been
347 recognized in other systems; for example, only a subset of aortic ECs respond to laminar flow[36].

348 Third, we were also surprised to find that Ca^{2+} is not required for histone-induced endothelial cell
349 deformation. Intracellular Ca^{2+} overload produced by any means, whether by SOCE or disruption of
350 membrane integrity, can destabilize cell membranes and lead to activation of cell death pathways[37]. The
351 peak timing of the histone-induced membrane changes (30-40 minutes) was later than when we observed
352 the Ca^{2+} surges (3-5 minutes). However, exposure to ionomycin, which elevates Ca^{2+} to a maximum level,
353 produced a different pattern of membrane activation from that of histones. Cells that are activated by
354 ionomycin did not show extensive membrane ruffling or retractions of lamellipodia, that we observed with
355 histone exposure. Rather, the endothelial response to ionomycin was characterized by a dramatic,
356 synchronous release of symmetrical (~5 μm diameter) membrane fragments across all cells. This pattern
357 appears consistent with exocytosis of preformed vesicles which likely represented Ca^{2+} dependent
358 exocytosis of Weibel-Palade bodies[38,39]. We also visualized extracellular vesicles being re-absorbed by
359 both adjacent and remote cells; extracellular vesicles were also passed between cells directly across
360 connected lamellipodia (Supplemental Video 12).

361 Surprisingly, exposure to histones in low Ca^{2+} exhibited an exaggerated response compared to
362 normal Ca^{2+} conditions (Figure 5). The patterns of dye entry and cellular deformation produced by histones
363 under low Ca^{2+} conditions matched those of normal Ca^{2+} but they were more extensive. The extent of
364 membrane thickening, blebbing, release of membrane fragments appeared visibly more extensive. This
365 was unexpected, because removal of extracellular Ca^{2+} prevents histone-induced endothelial cell Ca^{2+}
366 events[11] so it seemed plausible that Ca^{2+} overload would contribute to membrane effects. However, these
367 results were additionally confirmed by flow cytometry using FM1-43. Thus, low extracellular Ca^{2+}
368 concentrations make ECs more susceptible to histone-mediated membrane permeability.

369 In contrast, we also observed that elevated levels of extracellular Ca^{2+} could entirely block
370 membrane permeability in ECs. We also found that both high Ca^{2+} or Gd^{3+} blocked binding of GST-tagged
371 histone H3 to various membrane lipids, indicating that these compounds can interfere with histones binding
372 to the plasma membrane. Interestingly, only μM concentrations of Gd^{3+} were required to completely block
373 membrane permeability following histone exposure. In comparison, there was not a substantial block
374 observed by 1.2 mM Ca^{2+} levels which indicates the vast difference in neutralizing ability between these

375 two compounds. While both are highly cationic, Gd^{3+} binds more readily and strongly due to its higher
376 charge and greater charge density. These results support a model in which cationic histones bind the
377 negatively charged phospholipids in the cell surface through electrostatic interactions exacerbated when
378 during hypocalcemia due to loss of surface charge screening by calcium.

379 Finally, we found that high doses of histones lead to exposure of PS and uptake of viability dyes
380 after 1 hour. These findings align with prior literature on the endothelial cell toxicity of histones and their
381 ability to increase PS and activate pro-coagulatory changes [7,8,11,40,26]. Most notably, the exposure of PS
382 not only indicates endothelial activation, but could also represent a positive feedback loop in which histones
383 are more readily able to bind to the membranes of activated or pre-apoptotic cells. Since PS is a highly
384 negatively charged phospholipid that avidly binds histones (Figure 5), its presence on the outer leaflet of
385 the plasma membrane may cause pro-coagulatory or pre-apoptotic cells to become even more highly
386 susceptible to histone binding.

387 In addition to these findings, we also present novel evidence that a subset of endothelial cells can
388 recover from histone exposure. Although only a subset of histone-treated cells appeared to recover
389 membrane integrity (~15%) after 3 hours, this population is notable given that ionomycin-treated cells
390 consistently showed 0% recovery across all trials. These observations point to the existence of functionally
391 distinct subpopulations within the histone-treated group. It seems that histones may induce severe,
392 irreversible damage in a subset of highly susceptible cells while others experience a more moderate,
393 transient injury that permits membrane repair. Interestingly, a similar mosaic pattern of endothelial cell
394 calcium responses within a monolayer was reported in response to shear stress supporting the emerging
395 concept that a distinct subpopulation of cells within endothelial monolayers serve as sentinals that detect
396 and respond to local environmental cues[36].

397 In conclusion, our studies demonstrate that low Ca^{2+} levels enhance the interactions between
398 histones and endothelial cell membranes, leading to increased cytotoxicity. Conversely, elevated Ca^{2+}
399 levels – or treatment with agents that alter provide surface charge screening effects such as Gd^{3+} – block
400 histone-phospholipid interactions and mitigate endothelial damage. The effects of Ca^{2+} and Gd^{3+}, and lack

401 of effect with knocking out ORAI channels, support a model in which histone binding to cells occurs
402 primarily due to electrostatic interactions with negatively charged membranes.

403 Intravenous Ca^{2+} salts are used clinically, including during cardiac resuscitation and in
404 hyperkalemia. The stabilizing effects of Ca^{2+} on nerve and cardiac muscle cell membranes are usually
405 explained by the surface charge theory, in which higher Ca^{2+} levels decrease the density of the negative
406 charge surface near the sodium channel of myelinated nerve fibers, making it harder for sodium ions to
407 enter the cell and trigger an action potential[41,42]. For all cell types, the plasma membrane surface itself is
408 more electronegative than the lipid surface of cellular organelles, as shown by measurement of the binding
409 of prenylated cation probes[43]. That is because electric fields generated by cells depend not only on lipids
410 but also on ionizable components embedded in the external membrane surface. In vascular endothelial
411 cells, sugar moieties of the specialized glycocalyx confer additional net negative charge to the outer
412 surface[44]. This is critical to physiologic regulation of blood clotting, because the strong electronegative field
413 of the inner surface of blood vessels serves to repel the negatively charged circulating platelets and blood
414 components. In fact, early experiments showed that reversal of transmural potential across the aorta
415 produced gradual intravascular thrombus produces in complete aortic occlusion within 9 days, and
416 resulting biophysical models of charge characteristics were important in the development of vascular grafts
417 and surgical procedures[45,46]. However, the electric field generated by the net negative surface charge of
418 the vascular endothelium also serves to recruit extrinsic cationic proteins such as cytotoxic histones. We
419 show here that changes in the endothelial cell surface charge produced by elevated Ca^{2+} or by the addition
420 of Gd^{3+} to an extent sufficient to decrease the density of negative charge surface can screen membrane
421 phsopholipids from attracting cytotoxic histone proteins. This conclusion is supported by prior findings on
422 membrane dynamics and the mechanisms of histone cytotoxicity. For example, some proteins can bind to
423 the curved surface of cell membranes and thereby bend them, with resulting membrane deformations that
424 indirectly attract each other, producing membrane invaginations that lead to vesiculation[47]. This
425 phenomenon may partially explain the mode of action of histones. It is well known that histones are highly
426 cationic proteins that bind negatively charged phospholipids in bilayers and cell membranes[40,48–51], and
427 direct interactions between histones and cell membranes have been implicated in their toxic effects[8,52].

428 Recently, the globular domain of histones alone was shown to deform and lyse the lipid membranes of
429 liposomes and cultured ECs[40].

430 While the evidence strongly supports a model in which histone interacts with lipid bilayers directly,
431 independent of protein factors, the differences in responses among various cell types has not been
432 explained. For example, neurons are relatively insensitive to histones, compared to macrophages or ECs[53].
433 Our findings do not eliminate the possibly that extracellular histones have other important roles in innate
434 immune responses, for example, neutrophil-extracellular traps can serve to tether neutrophils to vascular
435 walls by binding von Willebrand factor[10,54]. Additionally, it has been shown that downstream immune or
436 pyroptotic responses can vary due to histone post-translational modifications, composition, DNA content,
437 and the cell type[8,48,52,55–57]. Prior literature has also implicated toll-like receptors 2 and 4 (TLR2 and TLR4),
438 the purinergic receptor P2X7, the receptor for advanced glycosylation end-products (RAGE), and/or direct
439 interaction between histones and membrane phospholipids[11,40,48,52,53,55,58–65]. It seems likely that histones
440 damage cells through multiple pro-inflammatory mechanisms, creating a cacophony of danger signals
441 which ultimately orchestrate cell death. Only through elucidating these synergistic pathways can we
442 understand why some ECs are susceptible to histones while others can withstand or even recover.

443 Our findings have clinical relevance to coagulopathy and endotheliopathy in shock and trauma.
444 Hypocalcemia occurs frequently during trauma resuscitation due to transfusion of citrated blood
445 products[14,15], but clinical protocols for massive transfusions diverge, with some recommending routine Ca^{2+}
446 administration while others recommend supplementation only as needed[16,17]. Moreover, it is important to
447 consider that, while we focused on ECs, other vascular cells are also sensitive to histones[63,52,56,58]. Future
448 studies will need to evaluate whether the previously reported histone toxicity to vascular smooth muscle
449 cells, erythrocytes, and platelets may also be increased in the presence of low Ca^{2+} conditions[63,64,64]; this
450 might have important implications in the context of resuscitation and massive transfusion protocols. In sum,
451 our results suggest that one of the dangers of untreated hypocalcemia is its potential to amplify histone-
452 induced endothelial injury, underscoring the importance of early and aggressive Ca^{2+} correction during
453 resuscitation. The development of standardized protocols to optimize Ca^{2+} administration in critically
454 injured patients has the potential to reduce the incidence of endotheliopathy and improve outcomes.

455 **Materials and Methods**

456 **Animal Husbandry.** Mice were kept on a 12 h light/dark cycle with ad libitum access to food and water
457 and were housed in groups of five. All studies were conducted in accordance with the Guidelines for the
458 Care and Use of Laboratory Animals (National Institute of Health) and approved by the Institutional Animal
459 Care and Use Committee of the University of Vermont.

460 **En Face Ca^{2+} Imaging.** En face murine vascular endothelial preparations were utilized for imaging as
461 previously described[11,30]. Briefly, adult male wildtype C57BL6j (C57) mice (Jackson Laboratories) were
462 euthanized using 5% Isoflurane, 95% O2, and decapitated. The mesentery was immediately harvested
463 and placed in 4°C HEPES-buffered physiological saline solution (HEPES-PSS: 10 mM HEPES, 134 mM
464 NaCl, 6 mM KCl, 1 mM $MgCl_2$, 2 mM $CaCl_2$, 7 mM glucose, pH 7.4). Mesenteric arteries (100-150 μm
465 internal diameter) were excised in sections of approximately 500 μm, cut longitudinally to expose the
466 lumen, and pinned flat with the endothelial surface exposed en face for imaging. Vessels were loaded with
467 green-fluorescent Ca^{2+} indicator (5 μM Cal-520 AM, Thermo Fisher Scientific) and incubated at 37 °C for
468 30 minutes prior to imaging

469 **Scanning Electron Microscopy.** Third order mesenteric arteries (~200 μm diameter) from male C57BL6/j
470 mice were cut open on one side longitudinally ("en face") and pinned down flat on a small silicone dish to
471 expose the intact endothelium. Arteries were incubated with 50 μg/mL of unfractionated histones (Sigma-
472 Aldrich, USA) for 30 minutes in HEPES-PSS (pH 7.4) at 37 °C. The arteries were then fixed in
473 paraformaldehyde (2%)-glutaraldehyde (2.5%) cacodylate buffer solution (0.1 M; pH 7.2) for 24 h, washed
474 with cacodylate buffer, post-fixed in a solution of 2.5% potassium ferrocyanide for 1 h, and washed again
475 in cacodylate buffer and ultrapure water. Sections were dehydrated in ascending grades of ethanol,
476 subjected to critical point drying in CO_2 (Samdri-PVT-3D, Tousimis, Rockville MD), coated with 10 nm of
477 pure gold in a vacuum sputter coater (Quorum EMS150R S, Electron Microscopy Sciences, Hatfield, PA)
478 and studied in a direct mode using a JEOL 6060 scanning electron microscope (Oxford Instruments, UK).

479 **Cultured cells.** Human endothelial (EA.hy926, ATCC) and kidney epithelial (HEK293, ATCC) cells were
480 cultured according to manufacturer instructions. Genetically engineered HEK 293 cells with a triple

481 knockout of ORAI1, ORAI2, and ORAI3 store-operated Ca^{2+} entry (SOCE) channels generated using
482 CRISPR-Cas9 gene editing as previously described[19].

483 **Live cell Ca^{2+} imaging.** Ca^{2+} events were recorded in cells before and after histone stimulation using the
484 Ca^{2+} indicators. HEK cells were loaded with Fura-2 and imaged with a plate reader. Cells were manually
485 identified and Ca^{2+} levels within each cellular region of interest were reported as the ratio of F_{340}/F_{380}. ECs
486 (EA.hy926 or mesenteric artery vascular preparations) were loaded with Cal-520 imaged using spinning
487 disk confocal microscopy. Ca^{2+} oscillations from movies were analyzed using automated custom software
488 (Volumetry, Grant Hennig) to create 2D and 3D prevalence maps allowing quantification of the numbers
489 of cells activated per field and the frequency, amplitude, and duration of Ca^{2+} events, as previously
490 described[30]. Ionomycin was applied at the conclusion of each experiment as a positive control which
491 maximally increased Ca^{2+} levels in all cells within the field of view[24].

492 **Live cell membrane imaging.** EA.hy926 cells were plated on glass coverslips and grown to ~70%
493 confluence. The coverslips were transferred to individual wells containing HEPES-PSS with no added Ca^{2+},
494 1.2 mM Ca^{2+}, or 12 mM Ca^{2+} as indicated. Membrane dye FM1-43 (2 μM) and Gd^{3+} (10 μM) – where
495 indicated – were added directly to the wells immediately prior to imaging. A baseline 3D Z-stack was then
496 acquired before the careful addition of 1 mL extra HEPES-PSS (vehicle control), 50 μg/mL histones or 10
497 μM ionomycin. Continuous 2D recordings were acquired at 1 frame per second for 40 minutes. Finally, a
498 second Z-stack was obtained. Individual cell cytoplasm ROIs were drawn manually in ImageJ, excluding
499 outer membrane signal at all timepoints. Fluorescence intensity was quantified for each cell as ΔF/F0 using
500 the following formula: $(F_t - F_{0min}) / F_{0min}$. For representative Z-stack images, .png files were loaded into
501 ImageJ and converted to 8-bit. Contrast was enhanced by lowering the maximum to 150 for each image
502 within ImageJ.

503 **Live cell viability imaging.** EA.hy926 cells were seeded at a density of 800,000 on 12 mm glass
504 coverslips and allowed to grow for 1-2 days prior to imaging. Hoechst 33342 (1 μg/mL) and SYTOX Green
505 (50 nM) were added to each well and incubated for 10 minutes at 37 °C in 5% CO_2. Coverslips were
506 washed three times with HEPES-PSS following staining. For baseline and post-stim timepoints, three fields
507 were imaged per coverslip, each consisting of a z-stack of 50 slices covering approximately 15-20 μm in

508 depth. Following baseline imaging, coverslips were transferred into stimulation wells containing either
509 HEPES-PSS control, histones (100 μg/mL) in HEPES-PSS, or ionomycin (10 μM) in HEPES-PSS. Cells
510 were incubated at 37 °C for 1 hour. At 50 minutes, SYTOX Green was added to the stimulation wells and
511 returned to the incubator. At the 1-hour mark, cells were imaged immediately (within 2-4 minutes),
512 acquiring three non-overlapping fields per coverslip. After imaging, coverslips were washed and transferred
513 into a recovery well pre-filled with 2 mL of media and returned to the incubator for a 3-hour recovery period.
514 After the 3-hour recovery in media, coverslips were removed, washed with HEPES-PSS, and placed in
515 fresh HEPES-PSS containing SYTOX AADvanced for 10 minutes before final imaging. For the final
516 timepoint, three fields per coverslip were imaged using a reduced stack depth of three slices (~15 nm).
517 **Flow Cytometry.** Cultured ECs were plated in 24-well tissue culture plates. Once cells were grown to
518 confluency, the media was aspirated off and replaced with HEPES-PSS buffer solution containing histones
519 as indicated. HEPES-PSS solutions contained no added Ca^{2+}, 1.2 mM Ca^{2+}, or 12 mM Ca^{2+} depending on
520 the condition. For membrane permeability assays, FM1-43 (2 μM) was added concurrently with histone
521 exposure and incubated with the cells for 40 minutes at 37 °C with 5%. The cells were then trypsinized,
522 centrifuged, and washed with phosphate buffered solution (PBS). For experiments evaluating cell viability,
523 cells were trypsinized and washed with PBS then resuspended in Annexin V binding buffer and stained
524 with Annexin V (Biolegend #640920) and Propidium Iodide (Thermo Fisher #2301111). Cells were
525 incubated at room temperature for 15 minutes prior to 1:5 dilution in binding buffer. Samples were run on
526 a flow cytometer (MACSQuant Analyzer 10, Miltenyi Biotec). Overall sample fluorescence was quantified
527 as the median fluorescent intensity (MFI); n of 3-4 for all conditions.
528 **Protein-Lipid Binding Assay.** Mega Lipid Strips (Echelon-Inc, Salt Lake City, UT) kits were used in
529 binding assays according to the manufacturer's instructions. Briefly, strips were blocked for one hour at
530 room temperature with 3% bovine serum albumin (BSA: Sigma-Aldrich, St. Louis, MO) in PBS-T
531 (phosphate buffered saline with 1% Tween-20). Strips were then incubated with Histone H3-GST (0.5
532 μg/mL; BPS Biosciences, San Diego, CA) for one hour at room temperature on an orbital shaker (170
533 RPM). Strips were then washed in PBS-T three times for 7 minutes each wash. Strips were then incubated
534 in 75 μL of a GST secondary antibody (Echelon-Inc, Salt Lake City, UT) for one hour at room temperature.

535 Strips were washed twice in PBS-T and twice in PBS for 5 minutes each. Strips were then incubated in 2
536 mL of TMB precipitating solution (Echelon-Inc, Salt Lake City, UT) for 2 minutes before imaging. Gd^{3+} (30
537 μM) was added during the blocking step prior to the addition of histones where indicated. Following
538 background subtraction, dot blot intensity was then quantified as area under the curve (AUC) using ImageJ
539 software.

540 **Data analysis and statistics.** GraphPad Prism software (ver. 10.4.0; GraphPad Software, USA) was
541 used for x–y graphing and analysis. Data were tested for normality using the Kolmogorov-Smirnov test.
542 Parametric t-test or ANOVA, or appropriate non-parametric alternatives were applied for comparisons
543 between groups, and differences were considered significant if $P < 0.05$.

544 <u>Ca^{2+} Fluorescence (Fura-2) Intensity.</u> Max peak intensity was quantified for each cell for the period of
545 stimulation. Since multiple measurements were taken from the same cell and compared across multiple
546 stimuli, matched values for each cell were stacked. For each trace, a two-way ANOVA was conducted to
547 compare the means across WT and ORAI TKO for each period of stimulation. Geisser-Greenhouse
548 correction was used for non-sphericity and Šidák correction was used to correct for multiple comparisons.

549 <u>Spatiotemporal Analysis of Ca^{2+} Fluorescence (Cal-520).</u> Data was quantified as the total area with Ca^{2+}
550 signals, normalized as a percent of the ionomycin response. Thus, each independent replicate generated
551 a percentage for baseline, Gd^{3+}, and histones. Two individual Friedman Tests for nonparametric, matched
552 data were conducted for the cultured and *en face* preps respectively.

553 <u>Lipid Binding.</u> The area under the curve (AUC) was quantified in ImageJ for each lipid dot. A two-way
554 ANOVA was used to compare histone-lipid binding for each lipid across different ionic conditions (0 mM
555 Ca^{2+}, 12 mM Ca^{2+}, 30 μM Gd^{3+}). Data points were stacked by replicate (n=3). Geisser-Greenhouse
556 correction was used for non-sphericity and Tukey correction was used to correct for multiple comparisons.

557 <u>Membrane Imaging.</u> Cell fluorescence (FM1-43) at 40 minutes was quantified as $\Delta F_{40min}/F0$. All individual
558 cell values were combined across replicates (n=3) and a Kruskal-Wallis test for non-parametric data was
559 performed. A threshold of greater than 1.0 $\Delta F_{40min}/F0$, representing 2-fold increase in fluorescence relative
560 to baseline, was used to calculate the percent of cells filled with dye at 40 minutes.

561 Flow Cytometry. MFI was quantified using the median fluorescent value for each histone replicate (n=3 or
562 4) and compared across ionic conditions (0 mM, 1.2 mM, 12 mM Ca^{2+}) using a Kruskal-Wallis test.
563 **Recovery Imaging Analysis.** Raw images were acquired using Fusion software and post-processed in
564 Imaris. Standard parameters were applied uniformly across all replicates to ensure consistency, including
565 four iterations of deconvolution and baseline subtraction using a 0.218 µm spatial threshold, as specified
566 in the software's baseline correction settings. Nuclear regions were identified based on the Hoechst 33342
567 signal. Using the Imaris classification tool, each nucleus was then assigned to a viability category – double-
568 positive (SYTOX $Green^{+}$/SYTOX $AADvanced^{+}$), SYTOX $Green^{+}$ only, SYTOX $AADvanced^{+}$ only, or
569 negative – based on fluorescence intensity and channel overlap within the defined nuclear region. This
570 approach ensured each cell was counted once and accurately categorized based on nuclear uptake alone.

571 **References**

572 1. Haagsma JA, Graetz N, Bolliger I, Naghavi M, Higashi H, Mullany EC, et al. The global burden of
573 injury: incidence, mortality, disability-adjusted life years and time trends from the Global Burden of
574 Disease study 2013. Inj Prev J Int Soc Child Adolesc Inj Prev. 2016 Feb;22(1):3–18.

575 2. Rudd KE, Johnson SC, Agesa KM, Shackelford KA, Tsoi D, Kievlan DR, et al. Global, regional, and
576 national sepsis incidence and mortality, 1990–2017: analysis for the Global Burden of Disease
577 Study. The Lancet. 2020 Jan 18;395(10219):200–11.

578 3. Aird WC. Phenotypic heterogeneity of the endothelium: I. Structure, function, and mechanisms. Circ
579 Res. 2007 Feb 2;100(2):158–73.

580 4. Johansson PI, Stensballe J, Ostrowski SR. Shock induced endotheliopathy (SHINE) in acute critical
581 illness - a unifying pathophysiologic mechanism. Crit Care Lond Engl. 2017 Feb 9;21(1):25.

582 5. Henriksen HH, McGarrity S, SigurÐardóttir RS, Nemkov T, D'Alessandro A, Palsson BO, et al.
583 Metabolic Systems Analysis of Shock-Induced Endotheliopathy (SHINE) in Trauma: A New
584 Research Paradigm. Ann Surg. 2020 Dec;272(6):1140–8.

585 6. Bunch CM, Chang E, Moore EE, Moore HB, Kwaan HC, Miller JB, et al. SHock-INduced
586 Endotheliopathy (SHINE): A mechanistic justification for viscoelastography-guided resuscitation of
587 traumatic and non-traumatic shock. Front Physiol. 2023;14:1094845.

588 7. Xu J, Zhang X, Pelayo R, Monestier M, Ammollo CT, Semeraro F, et al. Extracellular histones are
589 major mediators of death in sepsis. Nat Med. 2009 Nov;15(11):1318–21.

590 8. Abrams ST, Zhang N, Manson J, Liu T, Dart C, Baluwa F, et al. Circulating Histones Are Mediators of
591 Trauma-associated Lung Injury. Am J Respir Crit Care Med. 2013 Jan 15;187(2):160–9.

592 9. Johansson PI, Windeløv NA, Rasmussen LS, Sørensen AM, Ostrowski SR. Blood levels of histone-
593 complexed DNA fragments are associated with coagulopathy, inflammation and endothelial damage
594 early after trauma. J Emerg Trauma Shock. 2013 Jul;6(3):171–5.

595 10. Kolaczkowska E, Jenne CN, Surewaard BGJ, Thanabalasuriar A, Lee WY, Sanz MJ, et al. Molecular
596 mechanisms of NET formation and degradation revealed by intravital imaging in the liver vasculature.
597 Nat Commun. 2015 Mar 26;6:6673.

598 11. Collier DM, Villalba N, Sackheim A, Bonev AD, Miller ZD, Moore JS, et al. Extracellular histones
599 induce calcium signals in the endothelium of resistance-sized mesenteric arteries and cause loss of
600 endothelium-dependent dilation. Am J Physiol Heart Circ Physiol. 2019 01;316(6):H1309–22.

601 12. Shaw RJ, Abrams ST, Austin J, Taylor JM, Lane S, Dutt T, et al. Circulating histones play a central
602 role in COVID-19-associated coagulopathy and mortality. Haematologica. 2021 Sep 1;106(9):2493–
603 8.

604 13. Moore EE, Moore HB, Kornblith LZ, Neal MD, Hoffman M, Mutch NJ, et al. Trauma-induced
605 coagulopathy. Nat Rev Dis Primer. 2021 Apr 29;7(1):30.

606 14. Magnotti LJ, Bradburn EH, Webb DL, Berry SD, Fischer PE, Zarzaur BL, et al. Admission ionized
607 calcium levels predict the need for multiple transfusions: a prospective study of 591 critically ill
608 trauma patients. J Trauma. 2011 Feb;70(2):391–5; discussion 395-397.

609 15. Moore HB, Tessmer MT, Moore EE, Sperry JL, Cohen MJ, Chapman MP, et al. Forgot calcium?
610 Admission ionized-calcium in two civilian randomized controlled trials of prehospital plasma for
611 traumatic hemorrhagic shock. J Trauma Acute Care Surg. 2020 May;88(5):588–96.

612 16. DeBot M, Sauaia A, Schaid T, Moore EE. Trauma-induced hypocalcemia. Transfusion (Paris). 2022
613 Aug;62 Suppl 1:S274–80.

614 17. MacKay EJ, Stubna MD, Holena DN, Reilly PM, Seamon MJ, Smith BP, et al. Abnormal Calcium
615 Levels During Trauma Resuscitation Are Associated With Increased Mortality, Increased Blood
616 Product Use, and Greater Hospital Resource Consumption: A Pilot Investigation. Anesth Analg. 2017
617 Sep;125(3):895–901.

618 18. Shinde AV, Motiani RK, Zhang X, Abdullaev IF, Adam AP, González-Cobos JC, et al. STIM1 controls
619 endothelial barrier function independently of Orai1 and Ca2+ entry. Sci Signal. 2013 Mar
620 19;6(267):ra18.

621 19. Yoast RE, Emrich SM, Zhang X, Xin P, Johnson MT, Fike AJ, et al. The native ORAI channel trio
622 underlies the diversity of Ca2+ signaling events. Nat Commun. 2020 May 15;11(1):2444.

623 20. Emrich SM, Yoast RE, Xin P, Arige V, Wagner LE, Hempel N, et al. Omnitemporal choreographies of
624 all five STIM/Orai and IP3Rs underlie the complexity of mammalian Ca2+ signaling. Cell Rep. 2021
625 Mar 2;34(9):108760.

626 21. Emrich SM, Yoast RE, Trebak M. Physiological Functions of CRAC Channels. Annu Rev Physiol.
627 2022 Feb 10;84:355–79.

628 22. Trebak M, Bird GSJ, McKay RR, Putney JW. Comparison of human TRPC3 channels in receptor-
629 activated and store-operated modes. Differential sensitivity to channel blockers suggests
630 fundamental differences in channel composition. J Biol Chem. 2002 Jun 14;277(24):21617–23.

631 23. Koerdt SN, Gerke V. Annexin A2 is involved in Ca2+-dependent plasma membrane repair in primary
632 human endothelial cells. Biochim Biophys Acta Mol Cell Res. 2017 Jun;1864(6):1046–53.

633 24. Morgan AJ, Jacob R. Ionomycin enhances Ca2+ influx by stimulating store-regulated cation entry
634 and not by a direct action at the plasma membrane. Biochem J. 1994 Jun 15;300 (Pt 3)(Pt 3):665–
635 72.

636 25. Pereira LF, Marco FM, Boimorto R, Caturla A, Bustos A, De la Concha EG, et al. Histones interact
637 with anionic phospholipids with high avidity; its relevance for the binding of histone-antihistone
638 immune complexes. Clin Exp Immunol. 1994 Aug;97(2):175–80.

639 26. Bonson G, Lambert AR, Sackheim AM, Howard AJ, Piffard SH, Lescieur-Garcia C, et al.
640 ENDOTHELIAL-SPECIFIC KNOCKOUT OF THE SCRAMBLASE TMEM16F IMPAIRS IN VIVO
641 CLOT FORMATION. Shock Augusta Ga. 2025 May 1;63(5):788–95.

642 27. Johansson PI, Henriksen HH, Stensballe J, Gybel-Brask M, Cardenas JC, Baer LA, et al. Traumatic
643 Endotheliopathy: A Prospective Observational Study of 424 Severely Injured Patients. Ann Surg.
644 2017 Mar;265(3):597–603.

645 28. Rahbar E, Cardenas JC, Baimukanova G, Usadi B, Bruhn R, Pati S, et al. Endothelial glycocalyx
646 shedding and vascular permeability in severely injured trauma patients. J Transl Med. 2015 Apr
647 12;13:117.

648 29. Villalba N, Sackheim AM, Lawson MA, Haines L, Chen YL, Sonkusare SK, et al. The Polyanionic
649 Drug Suramin Neutralizes Histones and Prevents Endotheliopathy. J Immunol Baltim Md 1950. 2023
650 Aug 15;211(4):648–57.

651 30. Piffard SH, Hennig GW, Sackheim AM, Howard AJ, Lambert A, Majumdar D, et al. DISTINCT
652 PATTERNS OF ENDOTHELIAL CELL ACTIVATION PRODUCED BY EXTRACELLULAR
653 HISTONES AND BACTERIAL LIPOPOLYSACCHARIDE. Shock Augusta Ga. 2024 Nov
654 1;62(5):728–35.

655 31. Abdullaev IF, Bisaillon JM, Potier M, Gonzalez JC, Motiani RK, Trebak M. Stim1 and Orai1 mediate
656 CRAC currents and store-operated calcium entry important for endothelial cell proliferation. Circ Res.
657 2008 Nov 21;103(11):1289–99.

658 32. Fujii T, Sakata A, Nishimura S, Eto K, Nagata S. TMEM16F is required for phosphatidylserine
659 exposure and microparticle release in activated mouse platelets. Proc Natl Acad Sci. 2015 Oct
660 13;112(41):12800–5.

661 33. Suzuki J, Fujii T, Imao T, Ishihara K, Kuba H, Nagata S. Calcium-dependent Phospholipid
662 Scramblase Activity of TMEM16 Protein Family Members*. J Biol Chem. 2013 May
663 10;288(19):13305–16.

664 34. Schmaier AA, Anderson PF, Chen SM, El-Darzi E, Aivasovsky I, Kaushik MP, et al. TMEM16E
665 regulates endothelial cell procoagulant activity and thrombosis. J Clin Invest. 133(11):e163808.

666 35. Ashraf APK, Gerke V. Plasma membrane wound repair is characterized by extensive membrane lipid
667 and protein rearrangements in vascular endothelial cells. Biochim Biophys Acta Mol Cell Res. 2021
668 Jun;1868(7):118991.

669 36. Hong SG, Ashby JW, Kennelly JP, Wu M, Steel M, Chattopadhyay E, et al. Mechanosensitive
670 membrane domains regulate calcium entry in arterial endothelial cells to protect against
671 inflammation. J Clin Invest. 2024 May 21;134(13):e175057.

672 37. Orrenius S, Zhivotovsky B, Nicotera P. Regulation of cell death: the calcium-apoptosis link. Nat Rev
673 Mol Cell Biol. 2003 Jul;4(7):552–65.

674 38. Zupancic G, Ogden D, Magnus CJ, Wheeler-Jones C, Carter TD. Differential exocytosis from human
675 endothelial cells evoked by high intracellular Ca(2+) concentration. J Physiol. 2002 Nov
676 1;544(3):741–55.

677 39. Erent M, Meli A, Moisoi N, Babich V, Hannah MJ, Skehel P, et al. Rate, extent and concentration
678 dependence of histamine-evoked Weibel-Palade body exocytosis determined from individual fusion
679 events in human endothelial cells. J Physiol. 2007 Aug 15;583(Pt 1):195–212.

680 40. Pan Y, Peng M, Tong M, He Y, Hao M, Gao HL, et al. The Globular Domain of Extracellular Histones
681 Mediates Cytotoxicity via Membrane Disruption Mechanism. J Biol Chem. 2024 Nov 28;108038.

682 41. Hille B. Charges and potentials at the nerve surface. Divalent ions and pH. J Gen Physiol. 1968
683 Feb;51(2):221–36.

684 42. Hille B, Ritchie JM, Strichartz GR. The effect of surface charge on the nerve membrane on the action
685 of tetrodotoxin and saxitoxin in frog myelinated nerve. J Physiol. 1975 Aug;250(1):34P-35P.

686 43. Eisenberg S, Haimov E, Walpole GFW, Plumb J, Kozlov MM, Grinstein S. Mapping the electrostatic
687 profiles of cellular membranes. Mol Biol Cell. 2021 Feb 1;32(3):301–10.

688 44. Schmidt EP, Yang Y, Janssen WJ, Gandjeva A, Perez MJ, Barthel L, et al. The pulmonary
689 endothelial glycocalyx regulates neutrophil adhesion and lung injury during experimental sepsis. Nat
690 Med. 2012 Aug;18(8):1217–23.

691 45. Sawyer PN, Pate JW. Bio-electric phenomena as an etiologic factor in intravascular thrombosis. Am
692 J Physiol. 1953 Oct;175(1):103–7.

693 46. Sawyer PN. BIOELECTRIC PHENOMENA AND INTRAVASCULAR THROMBOSIS: THE FIRST 12
694 YEARS. Surgery. 1964 Nov;56:1020–6.

695 47. Reynwar BJ, Illya G, Harmandaris VA, Müller MM, Kremer K, Deserno M. Aggregation and
696 vesiculation of membrane proteins by curvature-mediated interactions. Nature. 2007 May
697 24;447(7143):461–4.

698 48. Kleine TJ, Lewis PN, Lewis SA. Histone-induced damage of a mammalian epithelium: the role of
699 protein and membrane structure. Am J Physiol. 1997 Dec;273(6):C1925-1936.

700 49. Pereira LF, Marco FM, Boimorto R, Caturla A, Bustos A, De la Concha EG, et al. Histones interact
701 with anionic phospholipids with high avidity; its relevance for the binding of histone-antihistone
702 immune complexes. Clin Exp Immunol. 1994 Aug;97(2):175–80.

703 50. Fürnrohr BG, Groer GJ, Sehnert B, Herrmann M, Voll RE. Interaction of histones with phospholipids--
704 implications for the exposure of histones on apoptotic cells. Autoimmunity. 2007 Jun;40(4):322–6.

705 51. Hariton-Gazal E, Rosenbluh J, Graessmann A, Gilon C, Loyter A. Direct translocation of histone
706 molecules across cell membranes. J Cell Sci. 2003 Nov 15;116(Pt 22):4577–86.

707 52. Silvestre-Roig C, Braster Q, Wichapong K, Lee EY, Teulon JM, Berrebeh N, et al. Externalized
708 histone H4 orchestrates chronic inflammation by inducing lytic cell death. Nature. 2019
709 May;569(7755):236–40.

710 53. Villalba N, Baby S, Cha BJ, Yuan SY. Site-specific opening of the blood-brain barrier by extracellular
711 histones. J Neuroinflammation. 2020 Sep 22;17(1):281.

712 54. Ward CM, Tetaz TJ, Andrews RK, Berndt MC. Binding of the von Willebrand factor A1 domain to
713 histone. Thromb Res. 1997 Jun 15;86(6):469–77.

714 55. Allam R, Scherbaum CR, Darisipudi MN, Mulay SR, Hägele H, Lichtnekert J, et al. Histones from
715 dying renal cells aggravate kidney injury via TLR2 and TLR4. J Am Soc Nephrol JASN. 2012
716 Aug;23(8):1375–88.

717 56. Vulliamy P, Gillespie S, Armstrong PC, Allan HE, Warner TD, Brohi K. Histone H4 induces platelet
718 ballooning and microparticle release during trauma hemorrhage. Proc Natl Acad Sci U S A. 2019
719 Aug 27;116(35):17444–9.

720 57. Marsman G, Zeerleder S, Luken BM. Extracellular histones, cell-free DNA, or nucleosomes:
721 differences in immunostimulation. Cell Death Dis. 2016 Dec 8;7(12):e2518.

722 58. Tsourouktsoglou TD, Warnatsch A, Ioannou M, Hoving D, Wang Q, Papayannopoulos V. Histones,
723 DNA, and Citrullination Promote Neutrophil Extracellular Trap Inflammation by Regulating the
724 Localization and Activation of TLR4. Cell Rep. 2020 May 5;31(5):107602.

725 59. Xu J, Zhang X, Monestier M, Esmon NL, Esmon CT. Extracellular histones are mediators of death
726 through TLR2 and TLR4 in mouse fatal liver injury. J Immunol Baltim Md 1950. 2011 Sep
727 1;187(5):2626–31.

728 60. Yang X, Li L, Liu J, Lv B, Chen F. Extracellular histones induce tissue factor expression in vascular
729 endothelial cells via TLR and activation of NF-κB and AP-1. Thromb Res. 2016 Jan 1;137:211–8.

730 61. Kleine TJ, Gladfelter A, Lewis PN, Lewis SA. Histone-induced damage of a mammalian epithelium:
731 the conductive effect. Am J Physiol. 1995 May;268(5 Pt 1):C1114-1125.

732 62. Kim J, Baalachandran R, Li Y, Zhang CO, Ke Y, Karki P, et al. Circulating extracellular histones
733 exacerbate acute lung injury by augmenting pulmonary endothelial dysfunction via TLR4-dependent
734 mechanism. Am J Physiol Lung Cell Mol Physiol. 2022 Sep 1;323(3):L223–39.

735 63. Semeraro F, Ammollo CT, Morrissey JH, Dale GL, Friese P, Esmon NL, et al. Extracellular histones
736 promote thrombin generation through platelet-dependent mechanisms: involvement of platelet TLR2
737 and TLR4. Blood. 2011 Aug 18;118(7):1952–61.

738 64. Semeraro F, Ammollo CT, Esmon NL, Esmon CT. Histones induce phosphatidylserine exposure and
739 a procoagulant phenotype in human red blood cells. J Thromb Haemost JTH. 2014 Oct;12(10):1697–
740 702.

741 65. Al-Aqtash R, Ross MS, Collier DM. Extracellular histone proteins activate P2XR7 channel current. J
742 Gen Physiol. 2023 Jul 3;155(7):e202213317.

743

744 **Figure Legends**

745 **Figure 1. Pre-treatment with Gd^{3+} blocks histone-induced Ca^{2+} signals independent of ORAI**
746 **channels.** (A) En face murine arteries were stained with fluorescent Ca^{2+} indicator (Cal-520, 5 μM) and
747 stimulated with histones (50 μg/mL) with or without Gd^{3+} (10 μM) pre-treatment- Representative,
748 cumulative Ca^{2+} prevalence images from continuous fields of view (FOV) showing surgically-opened
749 murine endothelium at baseline followed by 5 minutes of histone stimulation (top) or after pretreatment
750 withGd^{3+} followed by 5 minutes of histone stimulation. (B) Summary of Ca^{2+} activity in en face cells at
751 baseline compared to histone stimulation. (C) Summary of Ca^{2+} activity at baseline, after Gd^{3+} pre-
752 treatment, and during subsequent histone stimulation. Ca^{2+} signal was quantified as percent of the FOV
753 area with oscillating cells using a specialized standard deviation method, normalized to the ionomycin-
754 induced maximal response. (D) Wildtype (WT, left) and ORAI triple knockout (TKO, right) HEK 293 cells
755 were stained with Ca^{2+} indicator (Fura-2) and stimulated with histones (n=1). Ionomycin (10 μM) was added
756 at the end of each experiment as a positive control. Representative traces of fluorescence over time in
757 response to increasing concentrations of histones (top), pretreatment with Gd^{3+} (10 μM) followed by
758 histones (50 μg/mL) (middle), and Gd^{3+} (10 μM) post-treatment (bottom). Quantification of maximum peak
759 intensity for each cell following histone titration (E), Gd^{3+} pre-treatment (F), and Gd^{3+} post-treatment (G).

760 **Figure 2. Cultured ECs exhibit morphological changes and FM1-43 dye internalization in response**
761 **to histones and ionomycin over 40 minutes of exposure.** (A) Electron microscopy of native endothelial
762 cells exposed en face in murine blood vessels following exposure to histones (50 μg/mL) with arrows
763 pointing to areas of interest, including potential Weibel Palade bodies, retraction fibers, and blebs or
764 extracellular vesicles. (B) Representative images of cultured cells stained with membrane dye FM1-43
765 during exposure to buffered saline, histones (50 μg/mL), or ionomycin (10 μM). The same field of view is
766 presented at baseline (0 minutes), 20 minutes, and 40 minutes after exposure. (C) Magnification of
767 histone-stimulated and ionomycin-stimulated cells at 40 minutes, with arrows pointing to examples of bleb
768 formation on cell membranes.

769 **Figure 3. The patterns of plasma membrane movements produced by histones are different than**
770 **those caused by Ca^{2+} overload with ionomycin.** Examples of the distinct patterns of membrane

771 movements observed during video imaging of EC monolayers over a 60-minute time frame are presented
772 as both microscopy images and cartoons, with accompanying video supplements. (A) Ca^{2+} overload with
773 ionomycin caused similar changes in almost all cells across the field of view. The initial response consisted
774 of rapid membrane dye incorporation into the cytoplasm concomitant with the formation of small punctate
775 vesicular bodies located both intracellularly and in the bathing media. Following dye incorporation,
776 numerous filopodia were formed that elongated outwards from the cell body. These filopodia were motile
777 and not attached to the surface of the slide (A1: Supplemental Video 5). The formation of large blebs
778 marked the final response of cells before plasma membrane integrity was irrevocably lost (A2:
779 Supplemental Video 6). (B) Histone exposure produced a heterogenous, mosaic pattern in which some
780 cells respond rapidly and dramatically while others appear largely unaffected (Supplemental Video 7). Dye
781 uptake occurred in a patchy fashion in cells, often initiating at one or more regions before spreading
782 throughout the cell body. Extracellular vesicles appear to be both released and reabsorbed. Unique to the
783 histone response, membrane ruffling behavior was observed at the edges of some cells, with undulating
784 movements and expansion of the membrane border away from the cell body (B1: Supplemental Video 8)
785 whilst other cells underwent rapid retraction of the outer membrane (rounding), leaving behind retraction
786 fibers that remain connected to the media surface and adjacent cells (B2: Supplemental Video 9). A subset
787 of cells showed similar end-stage membrane movements with large amounts of blebbing and dye uptake
788 (B3: Supplemental Video 10). FOV Width = 490μm. Sub panel width = 70 – 97 μm.

789 **Figure 4. Histone-induced endothelial cell membrane deformation and lysis are exacerbated by low**
790 **Ca^{2+} and blocked by high Ca^{2+} or Gd^{3+}.** (A) Representative Z-stacks of cultured ECs after 40-minute
791 exposure to histones (50 μg/mL) under conditions of low (0 mM), normal (1.2 mM), or high (12 mM) Ca^{2+},
792 or with normal Ca^{2+} following Gd^{3+} (10 μM) pre-treatment. (B) Representative traces of individual cell
793 cytoplasmic fluorescence (ΔF/F0) over 40 minutes for each experimental condition, quantified using
794 ImageJ. (C) Final fluorescence ($\Delta F_{40min}/F0$) for each cell with replicates displayed separately (n=3) for each
795 condition. *Kruskal-Wallis test; P<0.05.*

796 **Figure 5. Histone-induced membrane permeabilization and membrane lipid binding can be**
797 **modulated by extracellular cation concentrations.** (A) Flow cytometry of histones on ECs shows

798 exacerbation of membrane permeabilization by low Ca^{2+} (0 mM) and block by high Ca^{2+} (12 mM).
799 Representative flow cytometry histograms showing FM1-43 fluorescence (PE) following incubation of
800 EA.hy926 cells with FM1-43 dye and 50 µg/mL histones or 10 µM ionomycin for 40 minutes in buffered
801 saline solution (HEPES-PSS) with zero added Ca^{2+} (0 mM), normal Ca^{2+} levels (1.2 mM), or high Ca^{2+} (12
802 mM). . The mean fluorescent intensity (MFI) was quantified using the median fluorescence for cells
803 exposed to 50 µg/mL histones at different Ca^{2+} concentrations. *Kruskal-Wallis test; P<0.05. (B)* Histone
804 H3 selectively binds to membrane bound lipids in a charge dependent manner. Representative images of
805 lipid binding strips exposed to histone H3 alone, in the presence of Gd^{3+} (30 µM), or in the presence of
806 Ca^{2+} (12 mM) (left). Schematic diagram of lipid identities, adapted from the manufacturer (Right; Echelon
807 Biosciences, Alabama, USA). (C) Summary data for histone H3 binding to cardiolipin, Phosphatidylinositol
808 4-phosphate (PtdIns(4)P), phosphatidic acid (PA), phosphatidylethanolamine (PE), Phosphatidylinositol
809 4,5-bisphosphate (PtdIns(4,5)P2), and phosphatidylserine (PS). phosphatidylcholine (PC), sphingomyelin,
810 and lysophosphocholine alone, or in the presence of Gd^{3+} (30 µM), or Ca^{2+} (12 mM). Binding was quantified
811 in ImageJ as Area Under the Curve (AUC). N=3 for each group. *Two-Way ANOVA with Bonferroni's*
812 *Correction for Multiple Comparisons; P<0.05.*

813 **Figure 6. High dose histone exposure induces a pre-apoptotic phenotype in ECs, which is**
814 **enhanced by low Ca^{2+} and blocked by high Ca^{2+}.** EA.hy926 cells were treated with histones (100 µg/mL)
815 in HEPES-PSS with 0, 1.2, or 12 mM Ca^{2+} for 1 hour, followed by Annexin V (PS) and Propidium Iodide
816 (PI) staining. (A) Representative flow cytometry histograms showing fluorescence of Annexin V (top) and
817 PI (bottom) for cells incubated in HEPES-PSS alone (blue) or with the addition of histones (pink). (B, C)
818 Median fluorescence intensity (MFI) for Annexin V and PI shown (n = 4). (D) Representative dot plots of
819 Annexin V and PI fluorescence. (E, F) Quantification of percent PS^{+}/PI^{-} cells and PS^{+}/PI^{+} cells using the
820 gating strategy shown in D.

821 **Figure 7. A subset of ECs with histone-induced membrane permeability can recover their**
822 **membrane integrity after 3 hours.** (A) Schematic diagram of experimental design allowing the
823 determination of four cell phenotypes following histone (100 µg/mL) or ionomycin (10 µM) stimulation: 1.
824 Intact ($Hoeschst^{+}$), 2. Late Permeability ($Hoeschst^{+}$ SYTOX-AADvanced^{+}), 3. Sustained Permeability

825 (Hoeschst^{+} SYTOX-AADvanced^{+} SYTOX Green^{+}), and 4. Recovered (Hoeschst^{+} SYTOX Green^{+}). (B)
826 Magnification of one representative field of view showing multiple permeability phenotypes following
827 histone stimulation for 1 hour and recovery for 3 hours. (C) Representative images from the post-recovery
828 timepoint for HEPES-PSS, histones, and ionomycin. Individual fluorescence channels are shown for
829 Hoeschst, SYTOX Green, and SYTOX AADvanced followed by a merge of all channels. (D) Cumulative
830 percentages of cells permeable to either SYTOX dye (SYTOX Green and/or SYTOX AADvanced) at
831 baseline, post-stimulation, and post-recovery for each treatment condition. (E) Percent of cells in each
832 phenotypic category at the post-recovery timepoint following stimulation with HEPES-PSS alone, histones,
833 or ionomycin.
834

835 **Supplemental Figure Legends**

836 **Supplemental Figure 1. Low-dose Gd^{3+} pre-treatment only partially blocks histone-induced Ca^{2+}**
837 **oscillations in HEK-293 cells, independent of ORAI channels.** Wildtype (WT, left) and ORAI triple
838 knockout (TKO, right) HEK-293 cells were stained with Ca^{2+} indicator (Fura-2) and stimulated with histones
839 (50 µg/mL, n=1). Ionomycin (10 µM) was added at the end of each experiment as a positive control. (A)
840 Representative traces of fluorescence over time in response to pretreatment with Gd^{3+} (5 µM) followed by
841 histones (50 µg/mL) for WT (left) and ORAI-TKO (middle). Quantification of maximum peak intensity for
842 each cell (right). (B) Representative traces of fluorescence over time in response to post-treatment with
843 Gd^{3+} (5 µM) followed by histones (50 µg/mL) for WT (left) and ORAI-TKO (middle). Quantification of
844 maximum peak intensity for each cell (right). (C) Representative traces of fluorescence over time in
845 response to histones (50 µg/mL) in 0 mM Ca^{2+} followed by 2 mM Ca^{2+} for WT (left) and ORAI-TKO (middle).
846 Quantification of maximum peak intensity for each cell (right). 2-way ANOVA for significance (n = 1 for
847 each experiment).

848 **Supplemental Figure 2. Moderate dose histones induce a subtle, pre-apoptotic phenotype in ECs,**
849 **which is enhanced by low Ca^{2+} enhances and blocked by high Ca^{2+} blocks.** EA.hy926 cells were
850 treated with histones (50 µg/mL) in HEPES-PSS with 0, 1.2, or 12 mM Ca^{2+} for 1 hour, followed by Annexin
851 V (PS) and PI staining. (A) Representative flow cytometry histograms showing fluorescence of Annexin V

852 (top) and PI (bottom) for cells incubated in HEPES-PSS alone (blue) or with the addition of histones (pink).
853 (B, C) Median fluorescence intensity (MFI) for Annexin V and PI shown (n = 4). (D) Representative dot
854 plots of Annexin V and PI fluorescence. (E, F) Quantification of percent PS^+/PI^- cells and PS^+/PI^+ cells
855 using the gating strategy shown in D.
856

857 **Supplemental Video Legends**

858 **Supplemental Video 1.** Histones induce Ca^{2+} influx in en face murine ECs. 3D representation of
859 cumulative Ca^{2+} oscillations over the 5 minute period after exposure to histones (50 µg/mL). Spatio-
860 temporal representation overlaid on 2D image of the same field of view with ionomycin-induced maximal
861 Ca^{2+} response.

862 **Supplemental Video 2.** Pretreatment with Gd^{3+} blocks histone-induced Ca^{2+} influx in en face murine ECs.
863 3D representation of cumulative Ca^{2+} oscillations after exposure to histones (50 µg/mL) in the presence of
864 Gd^{3+} (10 µM). Spatio-temporal representation overlaid on 2D image of the same field of view with
865 ionomycin-induced maximal Ca^{2+} response.

866 **Supplemental Video 3.** Video recording (25x) of ionomycin-induced endothelial cell membrane changes
867 visualized using the membrane dye FM1-43.

868 **Supplemental Video 4.** Video recording (25x) of histone-induced endothelial cell membrane deformation
869 visualized using the membrane dye FM1-43.

870 **Supplemental Video 5.** Full field of view with inset video of endothelial cell filopodia extrusion and
871 movement after application of ionomycin (30 minute recording: speed 96x).

872 **Supplemental Video 6.** Full field of view with inset video of endothelial cell membrane blebbing after
873 application of ionomycin (30 minute recording, speed 96x).

874 **Supplemental Video 7.** Full field of view with inset video of endothelial cell membrane ruffles after
875 application of histones (20 minute recording, speed 96x).

876 **Supplemental Video 8.** Full field of view with inset video of endothelial cell rounding after application of
877 histones (20 minute recording, speed 96x).

878 **Supplemental Video 9.** Full field of view with inset video of endothelial cell membrane blebbing after
879 application of histones (14 minute recording, speed 96x).
880 **Supplemental Video 10.** Video of histones-induced endothelial cell membrane ruffling (30 minute
881 recording, speed 96x).
882 **Supplemental Video 11.** Video of histone-induced endothelial cell membrane blebbing (30 minute
883 recording, speed 96x).
884 **Supplemental Video 12.** Video of ionomycin-induced release and reuptake of extracellular vesicles (30
885 minute recording, speed 96x).

Figure 1

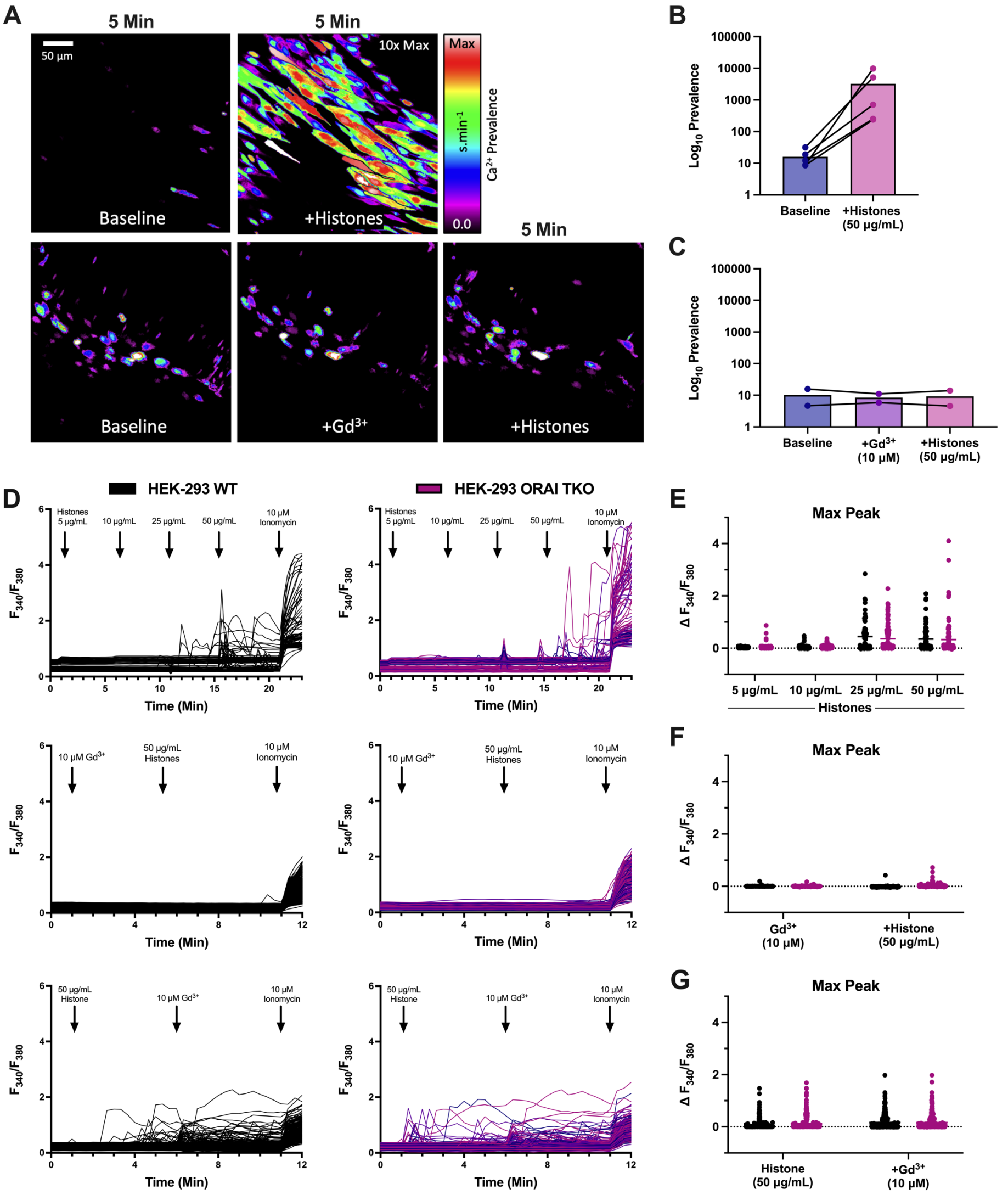
A
5 Min
5 Min
50 µm
10x Max
Max
s.min-1
0.0
Ca2+ Prevalence
Baseline
+Histones
5 Min
Baseline
+Gd3+
+Histones
B
Log10 Prevalence
Baseline
+Histones (50 µg/mL)
C
Log10 Prevalence
Baseline
+Gd3+ (10 µM)
+Histones (50 µg/mL)
D
HEK-293 WT
HEK-293 ORAI TKO
Histones 5 µg/mL
10 µg/mL
25 µg/mL
50 µg/mL
10 µM Ionomycin
10 µM Gd3+
50 µg/mL Histones
50 µg/mL Histone
F340/F380
Time (Min)
E
Max Peak
Δ F340/F380
5 µg/mL
10 µg/mL
25 µg/mL
50 µg/mL
Histones
F
Max Peak
Gd3+ (10 µM)
+Histone (50 µg/mL)
G
Max Peak
Histone (50 µg/mL)
+Gd3+ (10 µM)

Figure 2

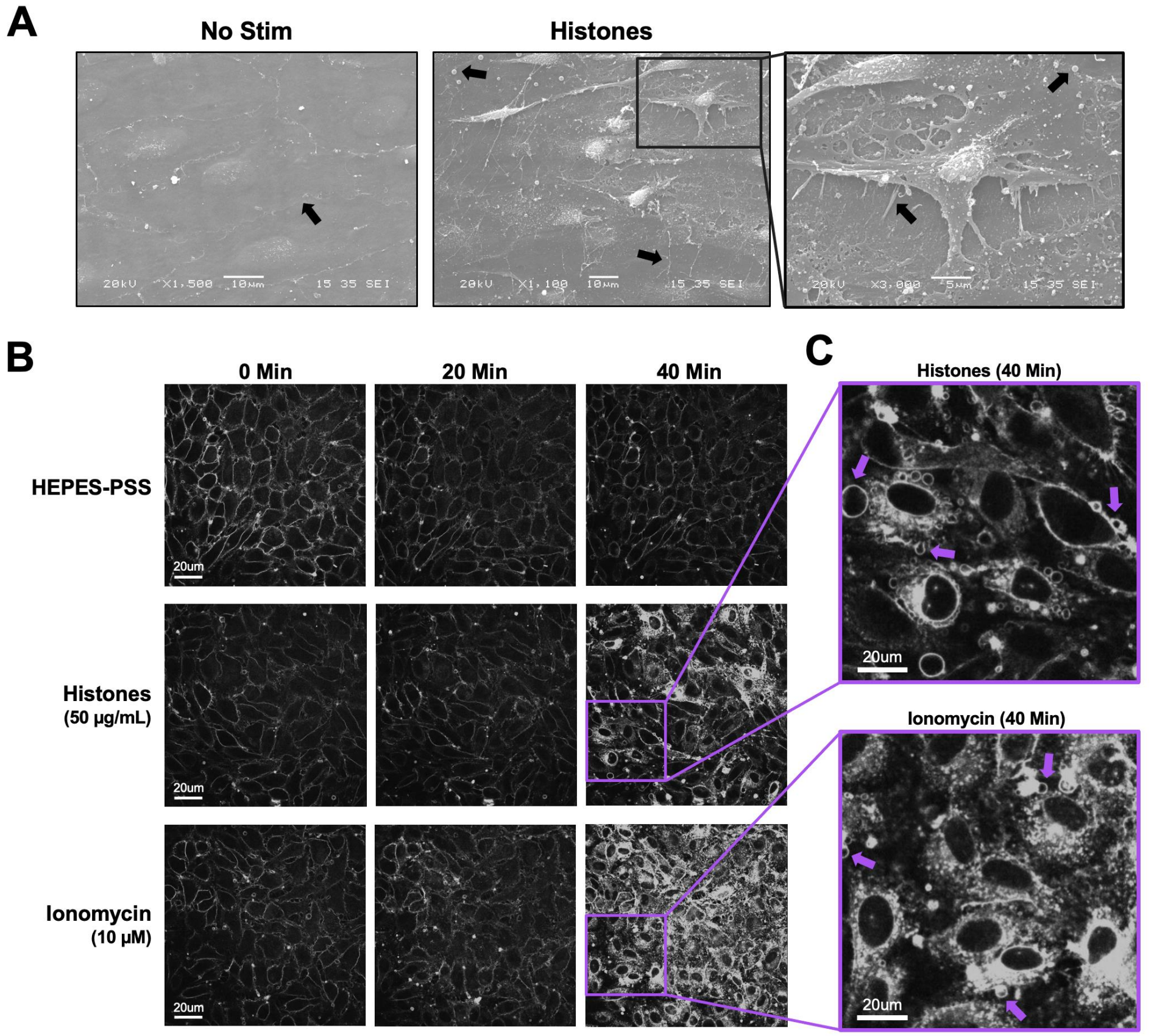
A
No Stim
Histones
20kV X1,500 10µm 15 35 SEI
20kV X1,100 10µm 15 35 SEI
20kV X3,000 5µm 15 35 SEI
B
0 Min
20 Min
40 Min
HEPES-PSS
Histones
(50 µg/mL)
Ionomycin
(10 µM)
20um
C
Histones (40 Min)
Ionomycin (40 Min)
20um

Figure 3

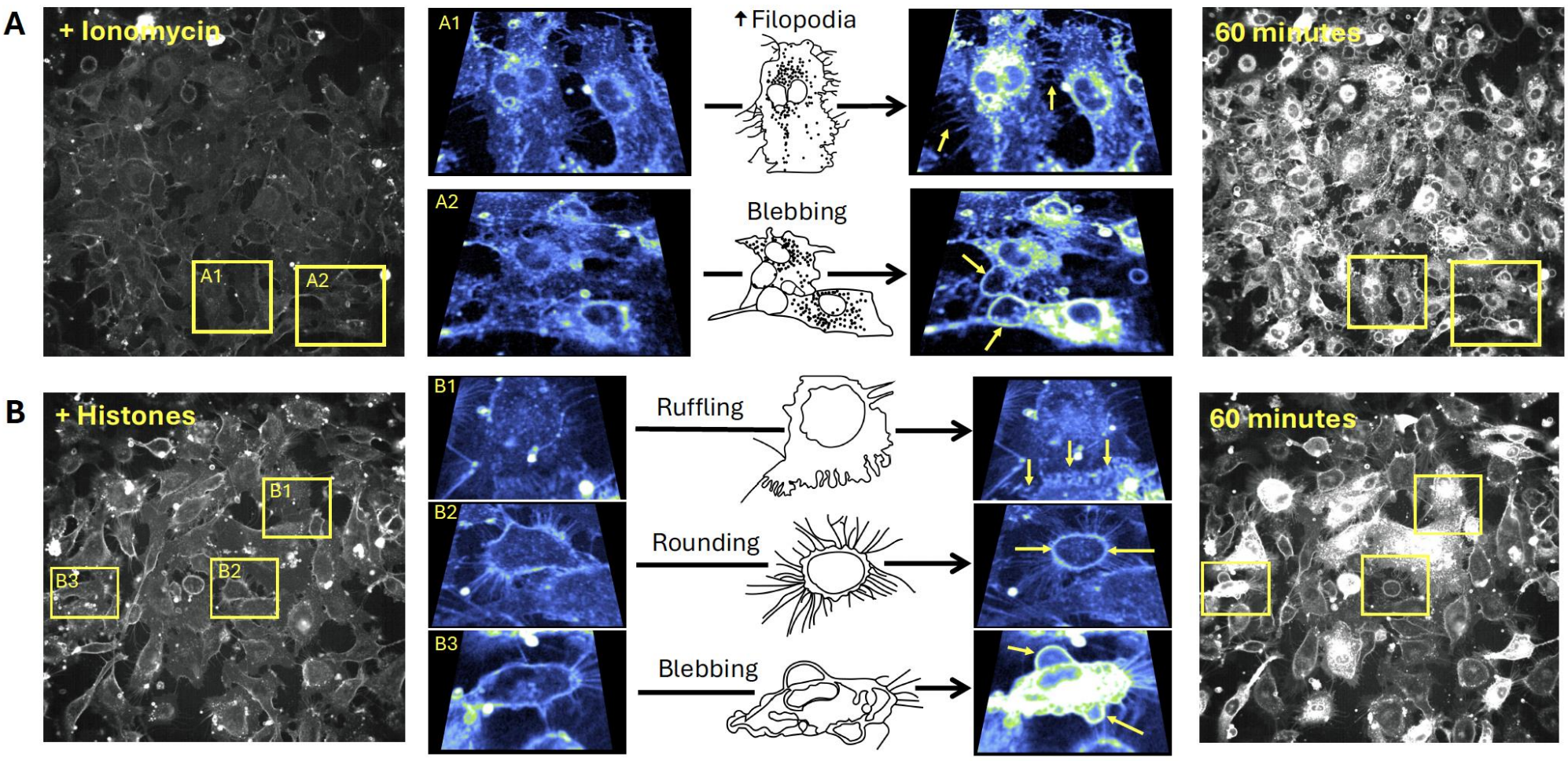
A
+ Ionomycin
A1
A2
A1
A2
Filopodia
Blebbing
60 minutes
B
+ Histones
B1
B2
B3
B1
B2
B3
Ruffling
Rounding
Blebbing
60 minutes

Figure 4

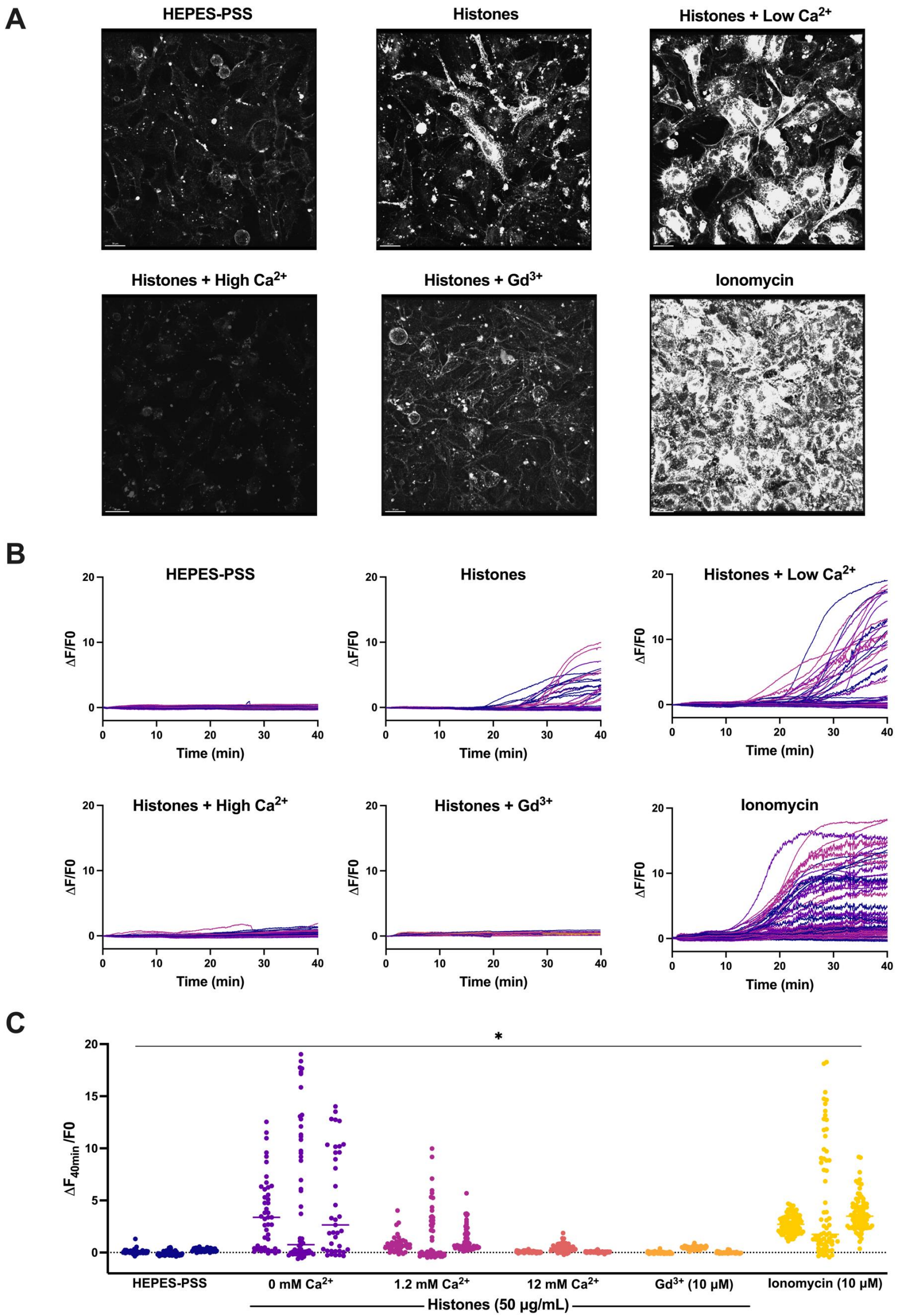
A
HEPES-PSS
Histones
Histones + Low Ca2+
Histones + High Ca2+
Histones + Gd3+
Ionomycin
B
HEPES-PSS
Histones
Histones + Low Ca2+
Histones + High Ca2+
Histones + Gd3+
Ionomycin
ΔF/F0
Time (min)
C
*
ΔF40min /F0
HEPES-PSS
0 mM Ca2+
1.2 mM Ca2+
12 mM Ca2+
Gd3+ (10 μM)
Ionomycin (10 μM)
Histones (50 μg/mL)

Figure 5

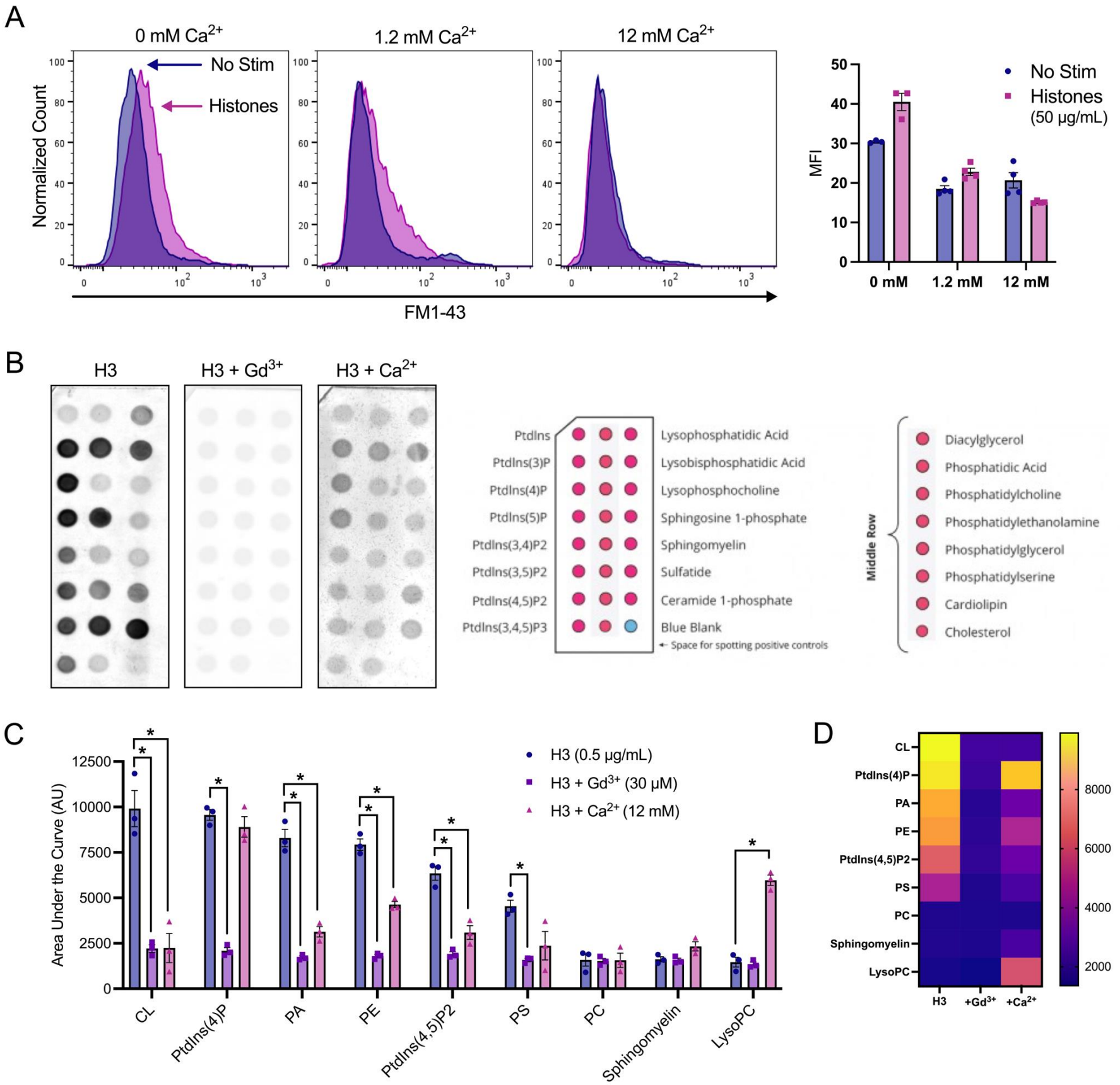
A
0 mM Ca2+
1.2 mM Ca2+
12 mM Ca2+
No Stim
Histones
Normalized Count
FM1-43
MFI
No Stim
Histones
(50 µg/mL)
0 mM
1.2 mM
12 mM
B
H3
H3 + Gd3+
H3 + Ca2+
PtdIns
PtdIns(3)P
PtdIns(4)P
PtdIns(5)P
PtdIns(3,4)P2
PtdIns(3,5)P2
PtdIns(4,5)P2
PtdIns(3,4,5)P3
Lysophosphatidic Acid
Lysobisphosphatidic Acid
Lysophosphocholine
Sphingosine 1-phosphate
Sphingomyelin
Sulfatide
Ceramide 1-phosphate
Blue Blank
Space for spotting positive controls
Middle Row
Diacylglycerol
Phosphatidic Acid
Phosphatidylcholine
Phosphatidylethanolamine
Phosphatidylglycerol
Phosphatidylserine
Cardiolipin
Cholesterol
C
H3 (0.5 µg/mL)
H3 + Gd3+ (30 µM)
H3 + Ca2+ (12 mM)
Area Under the Curve (AU)
CL
PtdIns(4)P
PA
PE
PtdIns(4,5)P2
PS
PC
Sphingomyelin
LysoPC
D
CL
PtdIns(4)P
PA
PE
PtdIns(4,5)P2
PS
PC
Sphingomyelin
LysoPC
H3
+Gd3+
+Ca2+

Figure 6

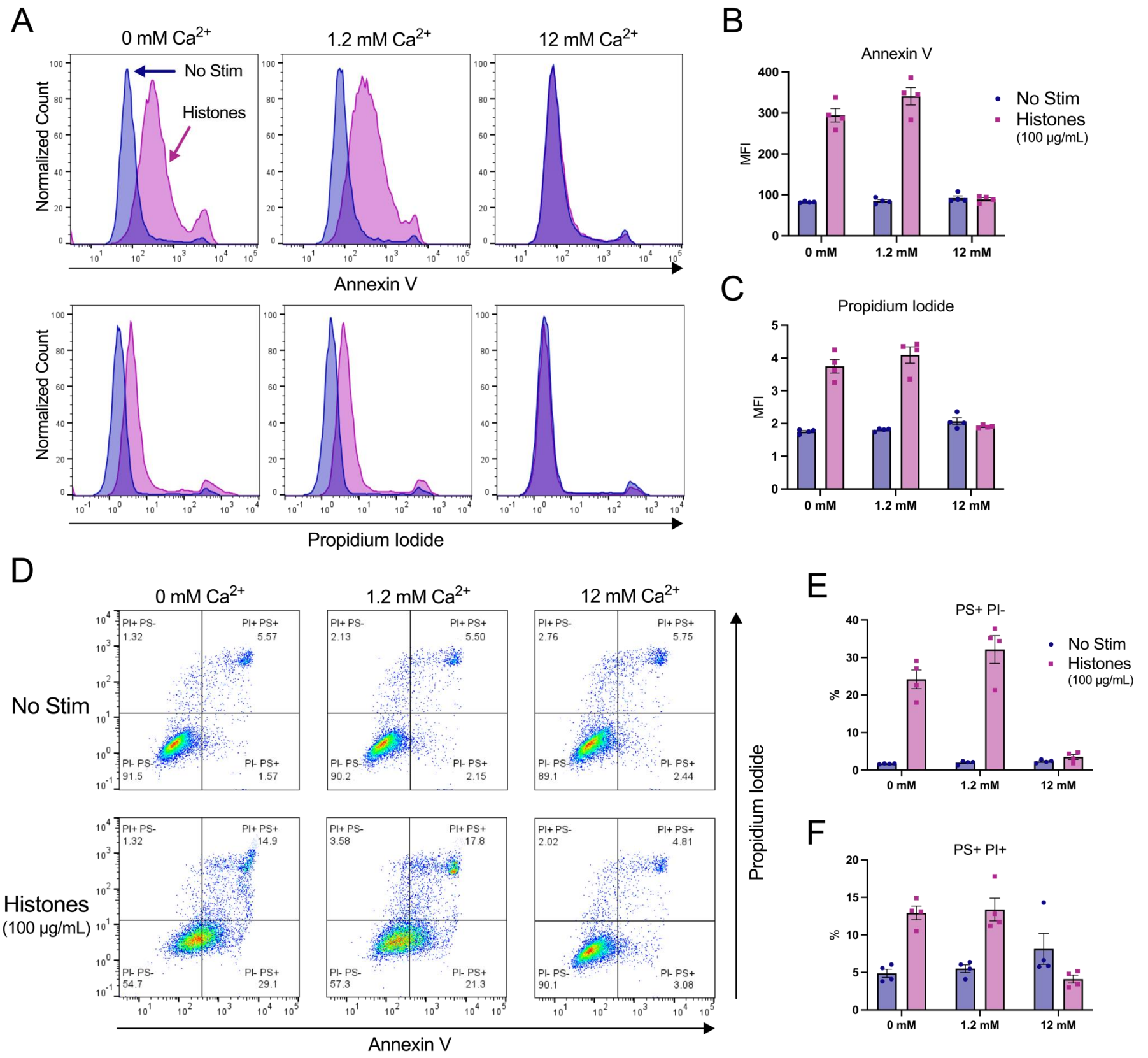
A
0 mM Ca2+
1.2 mM Ca2+
12 mM Ca2+
No Stim
Histones
Normalized Count
Annexin V
Propidium Iodide
B
Annexin V
MFI
No Stim
Histones
(100 µg/mL)
0 mM
1.2 mM
12 mM
C
Propidium Iodide
D
No Stim
Histones
(100 µg/mL)
PI+ PS-
PI+ PS+
PI- PS-
PI- PS+
1.32
5.57
91.5
1.57
2.13
5.50
90.2
2.15
2.76
5.75
89.1
2.44
14.9
54.7
29.1
3.58
17.8
57.3
21.3
2.02
4.81
90.1
3.08
E
PS+ PI-
%
F
PS+ PI+

Figure 7

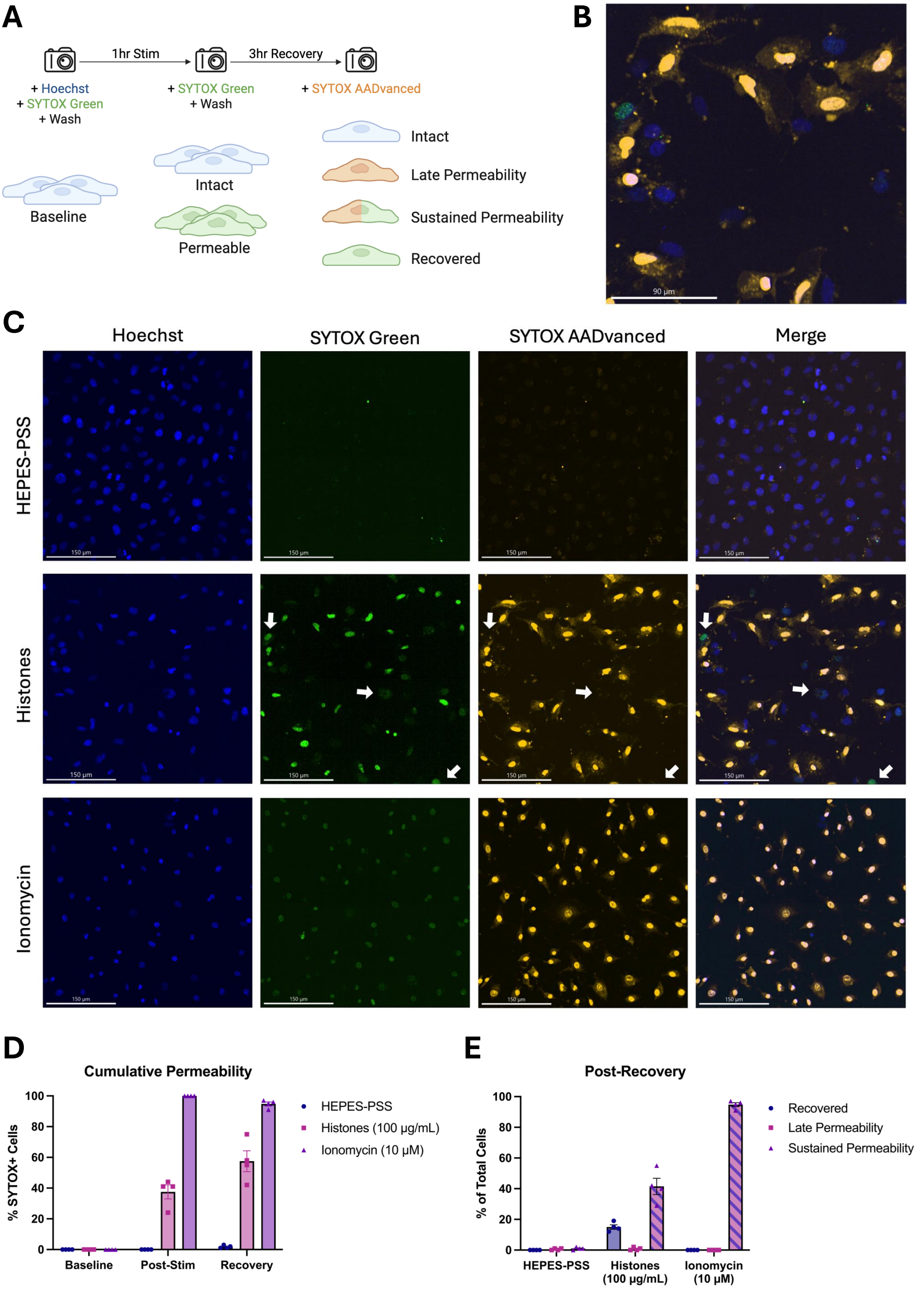
A
1hr Stim
3hr Recovery
+ Hoechst
+ SYTOX Green
+ Wash
+ SYTOX Green
+ Wash
+ SYTOX AADvanced
Baseline
Intact
Permeable
Intact
Late Permeability
Sustained Permeability
Recovered
B
90 µm
C
Hoechst
SYTOX Green
SYTOX AADvanced
Merge
HEPES-PSS
Histones
Ionomycin
150 µm
D
Cumulative Permeability
% SYTOX+ Cells
100
80
60
40
20
0
Baseline
Post-Stim
Recovery
HEPES-PSS
Histones (100 µg/mL)
Ionomycin (10 µM)
E
Post-Recovery
% of Total Cells
100
80
60
40
20
0
HEPES-PSS
Histones (100 µg/mL)
Ionomycin (10 µM)
Recovered
Late Permeability
Sustained Permeability